A Satellite Approach to Estimate Land–Atmosphere CO_2 Exchange for Boreal and Arctic Biomes Using MODIS and AMSR-E

John S. Kimball, *Member, IEEE*, Lucas A. Jones, *Student Member, IEEE*, Ke Zhang, Faith Ann Heinsch, Kyle C. McDonald, *Senior Member, IEEE*, and Walt C. Oechel

***Abstract*—Northern ecosystems are a major sink for atmospheric CO_2 and contain much of the world's soil organic carbon (SOC) that is potentially reactive to near-term climate change. We introduce a simple terrestrial carbon flux (TCF) model driven by satellite remote sensing inputs from the Moderate Resolution Imaging Spectroradiometer (MODIS) and the Advanced Microwave Scanning Radiometer for EOS (AMSR-E) to estimate surface ($<$ 10-cm depth) SOC stocks, daily respiration, and net ecosystem carbon exchange (NEE). Soil temperature and moisture information from AMSR-E provide environmental constraints to soil heterotrophic respiration (R_h), while gross primary production (GPP) information from MODIS provides estimates of the total photosynthesis and autotrophic respiration. The model results were evaluated across a North American network of boreal forest, grassland, and tundra monitoring sites using alternative carbon measures derived from tower CO_2 flux measurements and BIOME-BGC model simulations. Root-mean-square-error (rmse) differences between TCF model estimates and tower observations were 1.2, 0.7, and 1.2 $\mathbf{g \cdot C \cdot m^{-2} \cdot day^{-1}}$ for GPP, ecosystem respiration ($\mathbf{R_{tot}}$) and NEE, while mean residual differences were 43% of the rmse. Similar accuracies were observed for both TCF and BIOME-BGC model simulations relative to tower results. TCF-model-derived SOC was in general agreement with soil inventory data and indicates that the dominant SOC source for R_h has a mean residence time of less than five years, while R_h is approximately 43% and 55% of R_{tot} for respective summer and annual fluxes. An error sensitivity analysis determined that meaningful flux estimates could be derived under prevailing climatic conditions at the study locations, given documented error levels in the remote sensing inputs.**

***Index Terms*—Advanced Microwave Scanning Radiometer for EOS (AMSR-E), Arctic tundra, boreal forest, carbon, Moderate Resolution Imaging Spectroradiometer (MODIS), net ecosystem exchange (NEE).**

Manuscript received March 17, 2008; revised May 19, 2008 and June 17, 2008. First published December 2, 2008; current version published January 28, 2009. This work was supported in part by the National Aeronautics and Space Administration's Earth Science Enterprise and in part by the National Science Foundation's Office of Polar Programs through grants.

J. S. Kimball, L. A. Jones, and K. Zhang are with the Flathead Lake Biological Station, Division of Biological Sciences, The University of Montana (UM), Polson, MT 59860-6815 USA, and also with the Numerical Terradynamic Simulation Group, UM, Missoula, MT 59812 USA (e-mail: johnk@ntsg.umt.edu; lucas@ntsg.umt.edu; zhang@ntsg.umt.edu).

F. A. Heinsch is with the Numerical Terradynamic Simulation Group, The University of Montana, Missoula, MT 59812 USA (e-mail: faithann@ntsg.umt.edu).

K. C. McDonald is with the Water and Carbon Cycles Group, Science Division, Jet Propulsion Laboratory, California Institute of Technology, Pasadena, CA 91109 USA (e-mail: kyle.mcdonald@jpl.nasa.gov).

W. C. Oechel is with the Global Change Research Group, Department of Biology, San Diego State University, San Diego, CA 92182 USA (e-mail: oechel@sunstroke.sdsu.edu).

Color versions of one or more of the figures in this paper are available online at http://ieeexplore.ieee.org.

Digital Object Identifier 10.1109/TGRS.2008.2003248

NOMENCLATURE

AMSR-E	Advanced Microwave Scanning Radiometer for EOS.
BIOME-BGC	BIOME-BioGeochemical Cycles (BGC) model.
BPLUT	Biome property lookup table.
C_{met}, C_{str}, and C_{rec}	Metabolic, structural, and recalcitrant SOC pools, respectively.
GMAO	NASA Global Modeling and Assimilation Office.
GPP	Gross primary production (GPP $>$ 0 denotes photosynthetic uptake).
MODIS	Moderate Resolution Imaging Spectroradiometer.
MR	Mean residual error.
NCEP–NCAR	National Centers for Environmental Prediction–National Center for Atmospheric Research.
NEE	Net ecosystem carbon exchange (NEE $<$ 0 denotes ecosystem uptake).
NPP	Net primary production (NPP $>$ 0 denotes ecosystem uptake).
R_a	Autotrophic respiration ($R_a > 0$ denotes respiratory losses).
R_h	Heterotrophic respiration ($R_h > 0$ denotes respiratory losses).
rmse	Root-mean-square error.
R_{tot}	Total ecosystem respiration ($R_{\mathrm{tot}} > 0$ denotes respiratory losses).
SM	Soil moisture expressed as a proportion of relative saturation.
SOC	Soil organic carbon.
T_b	Microwave brightness temperature.
TCF	Terrestrial carbon flux model.

I. INTRODUCTION

NORTHERN high-latitude boreal and Arctic biomes are important components of the global carbon cycle because they constitute a major sink for anthropogenic CO_2 emissions and contain approximately 119 Pg of soil organic carbon (SOC) that is potentially reactive in the context of near-term climate change [1], [2]. Recent studies and long-term measurement records indicate that much of the region is becoming warmer [3] and drier [4]–[6] with recent declines in carbon sink strength

[7], [8]. Current and projected regional warming trends may exacerbate global climate change by destabilizing regional SOC stocks and reducing the capacity of northern ecosystems to sequester atmospheric CO_2.

The net ecosystem exchange (NEE) of carbon (CO_2) with the atmosphere is the residual difference between carbon uptake by vegetation gross primary production (GPP) and carbon loss through autotrophic and heterotrophic respiration, collectively termed ecosystem respiration. The NEE term is thus a useful measure of the magnitude and direction of carbon flow between ecosystems and the atmosphere [9]. Current capabilities for regional assessment and monitoring of NEE for boreal–Arctic ecosystems are limited. Atmospheric transport model inversions of CO_2 concentrations from sparse measurement stations provide information on seasonal patterns and trends in atmospheric CO_2 but little information on underlying processes; these methods are also too coarse to resolve carbon-source–sink activity at scales finer than broad latitudinal and continental domains [8], [10]. Tower CO_2 flux measurement networks provide detailed information on stand-level NEE and associated biophysical processes, but little information regarding spatial variability in these processes over heterogeneous landscapes [11]. Alternative measures of NEE and component carbon fluxes from satellite remote sensing potentially provide the means for scaling between relatively intensive stand-level measurement and modeling approaches, and top–down assessments from atmospheric model inversions.

The Moderate Resolution Imaging Spectroradiometer (MODIS) onboard the NASA EOS Terra and Aqua satellites has been providing global operational mapping of GPP at approximate eight-day intervals since 2000 and 2002, respectively [12]. The GPP term quantifies the photosynthetic uptake of atmospheric CO_2 but represents an incomplete picture of NEE because of a lack of information on ecosystem respiration. Several studies have applied satellite remote sensing to characterize NEE over boreal–Arctic landscapes using empirical relationships between CO_2 flux measurements and spectral vegetation indices [13], [14] or simple physiological models driven by optical–infrared (IR) remote sensing and surface meteorological data to characterize both vegetation productivity and ecosystem respiration [15], [16]. Empirical approaches are constrained to the specific regions and conditions under which they were developed and provide little diagnostic insight into underlying biophysical processes. Physiological models attempt to account for the primary environmental constraints on productivity and respiration but are often limited by the availability and resolution of driving meteorological data sets from sparse observational networks or coarse (1°–2.5°) resolution gridded products from atmospheric model reanalyses. Recent developments in satellite remote sensing offer the potential for direct measurement and improved resolution of environmental constraints for estimating land–atmosphere carbon exchange.

Satellite microwave radiometers are sensitive to variations in surface emissivity and dielectric constant associated with changes in soil moisture (SM) and temperature [17], [18]. Lower frequency microwaves (e.g., < 18.7 GHz) are capable of penetrating clouds and low-biomass vegetation to provide information more representative of the underlying soil than high frequency microwave and thermal IR observations. These favorable properties have been exploited for mapping surface SM and temperature across a wide range of environments and vegetation types, including boreal forest and tundra [19], [20]. The Advanced Microwave Scanning Radiometer for EOS (AMSR-E) is deployed with MODIS on the Aqua satellite and has been providing global multifrequency brightness temperature measurements on a daily basis since 2002. Current AMSR-E operational and experimental products include daily SM [18] and soil temperature [20], offering potential surrogate measures of SM and temperature controls to heterotrophic respiration. Thus, synergistic information from MODIS and AMSR-E may provide an alternative means for regional mapping and monitoring of NEE and component GPP and respiration fluxes. The relatively coarse ($\sim$25-km) spatial scale of the AMSR-E footprint limits the ability of the sensor to resolve subgrid-scale land surface properties. However, the utility of satellite microwave remote sensing for northern latitudes is the ability to monitor land surface conditions day or night, independent of solar illumination or signal degradation from cloud cover and other atmospheric aerosol effects.

We introduce a new satellite remote sensing algorithm for determining NEE and component carbon fluxes for boreal and Arctic ecosystems using synergistic biophysical information from MODIS and AMSR-E. Remote sensing inputs to the algorithm include land-cover class and GPP information from MODIS for characterizing general ecosystem properties and net photosynthetic uptake of CO_2, and daily surface soil temperature and moisture information from AMSR-E for estimating soil decomposition and heterotrophic respiration. A by-product of the algorithm initialization process includes a regional estimation of surface (< 10-cm depth) SOC stocks. The algorithm results are evaluated across a North American network of boreal forest, grassland (GRS), and tundra monitoring sites using independent measures of GPP, ecosystem respiration, and NEE derived from BIOME-BioGeochemical Cycles (BGC) ecosystem process model simulations and tower eddy covariance CO_2 flux measurements. The objectives of this paper are to characterize algorithm uncertainty and determine whether global operational satellite remote sensing products can be applied within a simple carbon model framework to determine NEE and component GPP and respiration fluxes with similar accuracy as more detailed ecosystem process model simulations.

II. Approach

A. Study Domain and Test Sites

We selected nine study sites for this investigation, encompassing North American tundra, boreal forest, and GRS ecosystems across a latitudinal climate and vegetation biomass gradient. The sites coincide with existing or previous tower eddy covariance CO_2 flux measurement campaigns and represent five distinct local vegetation types, including coastal wet-sedge tundra, moist tussock tundra, boreal evergreen needleleaf forest (ENLF), boreal deciduous broadleaf forest, and northern temperate GRS (see Table I and Fig. 1). The

TABLE I
BOREAL FOREST, GRASSLAND, AND TUNDRA STUDY SITES USED FOR TCF MODEL ASSESSMENT

Site	Site Abbrev.	MODIS[a] Land cover	Local vegetation[b]	Location (Lat. Lon.)
Barrow, AK	BRO	OSB	Wet-sedge tundra	71.32N 156.62W
Atqasuk, AK	ATQ	OSB	Tussock tundra	70.47N 157.40W
Prudhoe Bay, AK	UPD	OSB	Wet-sedge tundra	70.27N 148.88W
Happy Valley, AK	HPV	OSB	Tussock tundra	69.13N 148.83W
Ivotuk, AK	IVO	OSB	Tussock tundra	68.47N 155.73W
UAF-IARC near Fairbanks, AK	IARC	ENLF	Boreal spruce forest	64.87N 147.85W
NSA-OBS near Thompson, Manitoba CN	OBS	ENLF	Boreal spruce forest	55.88N 98.48W
SSA-OAS, Saskatchewan CN	OAS	MXF	Boreal aspen forest	53.63N 106.20W
Lethbridge, Alberta CN	LTH	GRS	Grassland	49.70N 112.93W

[a]Dominant vegetation classes within regional (25 km x 25 km) modeling windows as defined from a 1-km resolution MODIS IGBP global land cover classification [21], where OSB = Open shrubland; GRS = Grassland; ENLF = Evergreen needleleaf coniferous forest; MXF = Mixed broadleaf deciduous and evergreen needleleaf coniferous forest
[b]Dominant vegetation of tower CO_2 flux measurement footprints

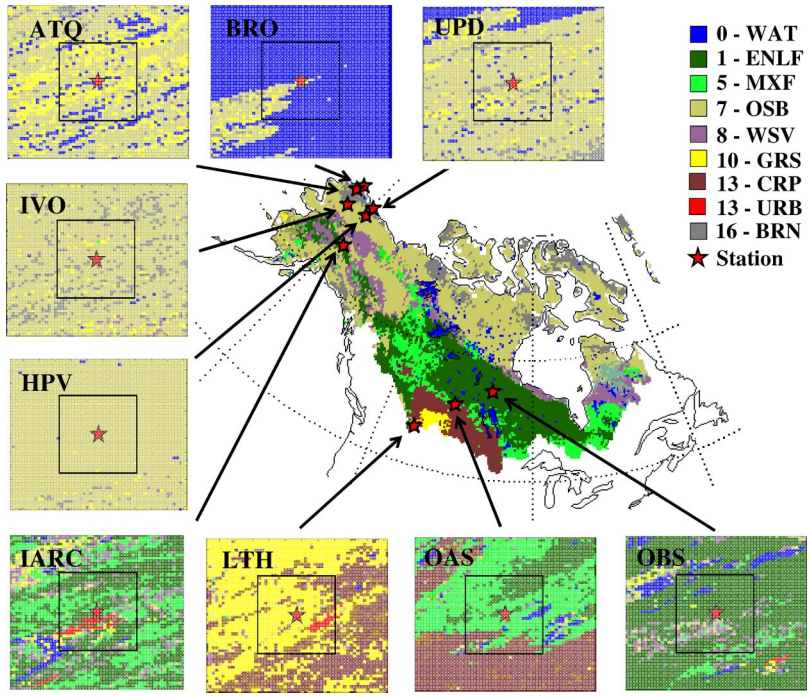

Fig. 1. North American study site locations with regional land cover defined by the MODIS International Geosphere–Biosphere Program (IGBP) land-cover classification mapped to a 25-km EASE grid format. The MODIS IGBP 1-km land cover is also presented for 25-km × 25-km modeling windows centered over each tower site, nested within larger 56-km × 56-km windows that reflect the relatively coarse AMSR-E T_B grid [20], [30]. The land-cover categories include WAT, ENLF, MXF, OSB, woody savannah (WSV), GRS, CRP, urban (URB), and barren or sparsely vegetated land (BRN).

BRO and UPD sites are dominated by coastal wet-sedge tundra and are characterized by low topography and a shallow water table with numerous thaw lakes [22]–[24]. The vegetation is predominantly composed of low-growing herbaceous sedges, grasses, mosses, and lichens, interspersed with areas of shallow standing water. The Gelisol soils are highly organic and consist of a shallow active layer that thaws each growing season and is underlain by continuous permafrost. The IVO, ATQ, and HPV sites are characterized by moist tussock tundra dominated by *Eriophorum vaginatum* and low forbs and shrubs composed of both deciduous and evergreen species [23], [25]. These sites are located on upland tundra where the soil active layer tends to be thicker than that of coastal sites.

The boreal OBS and IARC sites are composed of mature of black spruce (*Picea mariana*) stands with respective overstory canopy heights ranging from 10 to 13 m and 1.5 to 6 m, and low topographic relief with discontinuous permafrost [26], [27]. The IARC understory is composed of a nearly continuous cover of mosses (*Pleurozium* and *Hylocomium* spp.) with a thick (~20-cm) organic matter layer and Gelisol soils. Vegetation in the vicinity of the OBS tower includes aspen (*Populous tremuloides*) and jack pine (*Pinus banksiana*) stands on well-drained soils, black spruce and feathermoss (*Pleurozium* spp.) on moderately drained soils, and black spruce and a thick layer of mosses (*Sphagnum* spp.) on poorly drained soils. The boreal OAS site is dominated by a mature aspen (*Populus tremuloides*) overstory with a mean canopy height of 21 m and low topographic relief [28]. The OAS site also contains an extensive understory predominantly composed of hazelnut (*Corylus cornuta* Marsh.) with medium-to-fine silty-clay-textured Gray Luvisol (Alfisol) soils. The LTH site is the southernmost study site and is composed of semiarid short-grass prairie on relatively flat terrain [29]. Vegetation is dominated by grasses (*Agropyron* spp.) with a mean canopy height of approximately 18 cm. Soils

at the LTH site are composed of orthic dark-brown chernozems (Mollisols) with a clay loam texture.

We identified the dominant land-cover class within overlying 25-km × 25-km windows surrounding each site location using the MODIS IGBP global land-cover classification [21]. In most cases, the local vegetation was of a similar functional type as the overlying global land-cover classification. The tundra sites were identified as open shrubland (OSB) by the land-cover classification. The BRO_1 and BRO_2 tower locations are within 1 km of each other and were represented within the same regional window. The OBS and IARC sites were classified as ENLF, while the LTH site was classified as GRS. The aspen-dominated OAS tower footprint differed from the regional land cover, which was classified as mixed evergreen needleleaf and broadleaf deciduous forest (MXF) due to the relative abundance of both vegetation functional types within the regional modeling window.

B. Model Development

We applied a simple terrestrial carbon flux (TCF) model to compute ecosystem respiration and NEE on a daily basis. Our approach has structural elements similar to the Century [31], [32] and CASA [33] soil decomposition models but is adapted for use with daily biophysical inputs derived from both satellite optical–IR and passive microwave remote sensing time series as primary model drivers. Model inputs include daily GPP, soil temperature, and SM. GPP is used to estimate vegetation net primary production (NPP), autotrophic respiration, and metabolic, structural, and recalcitrant SOC pools. Surface ($<$ 10-cm depth) soil temperature and moisture inputs are used to define the environmental controls to soil decomposition and heterotrophic respiration. Static inputs to the model include a global land-cover classification, which is used within the framework of a general biome properties lookup table (BPLUT) to define physiological response characteristics of different vegetation classes. All model inputs represent satellite-remote-sensing-derived products from NASA EOS sensors.

NEE (in grams of carbon per square meter per day) is computed on a daily basis as the residual difference between GPP and respiration from autotrophic (R_a) and heterotrophic (R_h) components

$$\text{NEE} = (R_a + R_h) - \text{GPP} \tag{1}$$

where positive $(+)$ and negative $(-)$ NEE fluxes denote the respective terrestrial loss or uptake of CO_2. The GPP term (in grams of carbon per square meter per day) represents the mean vegetation GPP of the dominant land-cover class within a grid cell and is obtained as an external model input. The R_a term encompasses growth and maintenance respiration components and is computed on a daily basis as a fixed proportion of GPP within individual land-cover classes, based on observational evidence that the ratio of R_a to GPP is conserved across global biomes [34]–[36]. While this assumption provides a key simplification for a remote sensing algorithm, the proportion of plant photosynthesis devoted to biophysical growth and maintenance may vary under changing environmental conditions and over the course of vegetation development [37]–[39].

Heterotrophic respiration is computed as the sum of variable decomposition and respiration rates from three distinct carbon pools as

$$R_h = (K_{\text{met}}C_{\text{met}} + K_{\text{str}}C_{\text{str}} + K_{\text{rec}}C_{\text{rec}}) \tag{2}$$

where C_{met}, C_{str}, and C_{rec} (in grams of carbon per square meter) represent metabolic, structural, and recalcitrant SOC pools, and K_{met}, K_{str}, and K_{rec} (per day) are the corresponding decomposition rate parameters. The metabolic and structural SOC pools represent plant litter with relatively short (e.g., less than or equal to five years) turnover periods, while the recalcitrant pool represents more physically and chemically protected SOC with a longer turnover time.

The three-pool soil decomposition model approach is a simple approximation of the complex variation of intrinsic SOC turnover rates but has been found to produce results consistent with a wide range of observations from soil warming and incubation experiments [40]. Annual inputs to the C_{met} and C_{str} pools in (2) are derived as proportions of annual NPP, and input to C_{rec} is a constant fraction of the C_{str} pool; outputs to these SOC pools represent the annual sums of respired components from (2)

$$dC_{\text{met}}/dt = C_{\text{fract}}\text{NPP} - R_{h,\text{met}} \tag{3}$$

$$dC_{\text{str}}/dt = (1 - C_{\text{fract}})\text{NPP} - 0.7\,C_{\text{str}} - R_{h,\text{str}} \tag{4}$$

$$dC_{\text{rec}}/dt = 0.7\,C_{\text{str}} - R_{h,\text{rec}} \tag{5}$$

where NPP is estimated as a fixed proportion of annual GPP (in grams of carbon per square meter per year) for individual land-cover classes, based on the assumption of conservatism in vegetation-carbon-use efficiency (i.e., NPP/GPP) and the proportional allocation of GPP to R_a within global biomes [34]–[36]. The C_{fract} term defines the rate in which NPP is allocated to metabolic and structural SOC pools, and is specified as a fixed rate within individual land-cover classes [32], [33]. Values for C_{fract}, and proportional allocations of GPP to R_a and NPP are defined in a BPLUT of general ecophysiological properties of each land-cover class (Table II). This approach is based on the assumption that the litter input to the SOC pool is proportional to NPP under long-term steady-state conditions [31], [32].

The TCF model uses dimensionless rate curves to account for soil temperature and moisture constraints to soil decomposition. The soil decomposition rate (K) is derived as the product of dimensionless multipliers for soil temperature (T_{mult}) and moisture (W_{mult}) and a theoretical maximum rate constant (K_{mx}; per day) under prevailing climate conditions

$$K = K_{\text{mx}}T_{\text{mult}}W_{\text{mult}} \tag{6}$$

where K is equivalent to K_{met}, and T_{mult} and W_{mult} vary between zero and one. The value for K_{mx} was specified as a constant rate (0.0301 per day) for all biomes, while decomposition rate parameters for K_{str} and K_{rec} were estimated as 40% and 1% of K_{met}, respectively [32]. The estimation of K in (6)

TABLE II
GENERAL BPLUT DESCRIBING SITE ECOPHYSIOLOGICAL PARAMETERS FOR TCF MODEL CALCULATIONS

Site	C_{fract} (DIM)[a]	CUE (DIM)[b]	R_a:GPP (DIM)[b]
BRO	0.72	0.54	0.46
ATQ	0.72	0.54	0.46
UPD	0.72	0.54	0.46
HPV	0.72	0.54	0.46
IVO	0.72	0.54	0.46
IARC	0.49	0.54	0.46
OBS	0.49	0.54	0.46
OAS	0.59	0.54	0.46
LTH	0.76	0.6	0.4

[a]Proportional NPP allocation to metabolic and structural (1-C_{fract}) SOC pools for boreal forest, grassland and tundra biomes from[32] and [33]
[b]Carbon Use Efficiencies (NPP:GPP) and corresponding R_a:GPP ratios for representative boreal and grassland ecosystems from [35]

assumes constant soil decomposer efficiency (microbial-CO_2-production-to-carbon-assimilation ratio) inherent in the $K_{\rm mx}$ term, and that SM and temperature are the dominant controls on near-term (daily, seasonal, and annual) decomposition rates. However, we assume that changes in litter quality (e.g., physical protection and/or chemical resistance to microbial decomposition) influence R_h and NEE indirectly through associated changes in satellite-remote-sensing-derived GPP inputs over generally N-limited boreal and tundra ecosystems.

The soil decomposition rate response to temperature is defined using an Arrhenius-type function following [41]

$$T_{\rm mult} = \exp\left[308.56\left((66.02)^{-1} - (T_{s,k} - 227.13)^{-1}\right)\right] \quad (7)$$

where (7) is expressed relative to a 20-°C reference temperature and $T_{s,k}$ is the surface soil temperature (in kelvins). A variety of functional types have been used to describe temperature effects on soil respiration, including exponential [42], [43] and Poisson [31], [32] functions, while the Arrhenius functional type is physically based and provides a relatively accurate and unbiased estimate of soil respiration across a wide range of biome types and environmental conditions [40], [41], [44]. We assume that for soil temperatures above a 20-°C reference state, $T_{\rm mult}$ is unity, and temperature is no longer limiting to soil decomposition. Under these conditions, SM is expected to decline with warmer soil temperatures, and $W_{\rm mult}$ becomes the primary constraint to K.

The soil decomposition rate response to SM has been described using quadratic and parabolic functions and varying expressions of soil water content, with optimum rates being at intermediate soil water levels [45]. For this investigation, the soil decomposition rate response to SM is represented as a parabolic function

$$W_{\rm mult} = 0.00036(105.0\ {\rm SM} - {\rm SM})^2 \quad (8)$$

where SM is expressed as a proportion (in percent) of saturation. The parabolic response curve accounts for the inhibitory effects of both low and high soil water on heterotrophic respiration rates and is consistent with laboratory soil incubation studies and field observations for a range of global biome types, including GRS and tundra [46]–[49]. The SM limitation to decomposition described by (8) approaches unity near 50% of soil saturation, although the shape of the parabolic response is likely to vary across different biomes and soil types. For this investigation, we assume that mean surface soil properties within boreal and arctic biomes are similar at the relatively coarse (∼25-km) spatial resolution of satellite-microwave-remote-sensing-derived SM inputs.

C. TCF Model Inputs

The TCF model requires time series inputs of daily GPP, surface soil temperature, and SM to compute ecosystem respiration and NEE on a daily basis. Model inputs were derived using a three-year (2002–2004) daily time series of GPP, soil temperature, and SM derived from MODIS and AMSR-E sensor records. A MODIS global land-cover classification [21] was used with the BPLUT in Table II to define general ecophysiological properties for each of the study sites; the BPLUT parameters were derived from the literature for boreal, GRS, and tundra ecosystems. For each site window, the $C_{\rm met}$, $C_{\rm str}$, and $C_{\rm rec}$ pools were initialized to steady-state conditions by continuous cycling of the three-year GPP, soil temperature, and SM daily time series.

1) GPP: The NASA MODIS has been operational on the NASA EOS Terra and Aqua satellites since 2000 and 2002, respectively, and provides a variety of consistent, well-calibrated, and validated land surface information ranging from spectral radiance and reflectance data to derived higher order biophysical variables including land-cover type, canopy photosynthetic leaf area, and vegetation productivity. Model GPP inputs were derived from the MODIS MOD17A2 algorithm [12]. The MOD17A2 algorithm has undergone several major revisions in response to extensive ongoing calibration and verification studies using biophysical information from regional station networks, including boreal and Arctic landscapes (e.g., [50]–[53]). For this investigation, we use the fifth-generation (Collection 5) version of the MOD17A2 algorithm and associated MOD15 LAI and FPAR inputs [52], [54]. The MOD17A2 algorithm uses a production efficiency model with MODIS sensor-derived land cover, fractional photosynthetically active radiation (FPAR), leaf area index (LAI), and daily surface meteorology as primary drivers. Daily surface meteorology inputs include incident solar radiation ($SW_{\rm rad}$), minimum and mean daily air temperatures ($T_{\rm min}$ and $T_{\rm avg}$, respectively), and atmospheric vapor pressure deficit (VPD), which are provided by the NASA Global Modeling and Assimilation Office (GMAO) reanalysis surface meteorology [55], [56]. The surface meteorological data are used with simple response curves to estimate environmental reductions in photosynthetic-light-use efficiency under suboptimal solar radiation, temperature, and humidity conditions. The biophysical characteristics of the land surface vary according to individual land-cover classes as defined using a 1-km-resolution global land-cover map and the MOD17A2 BPLUT [52]. GPP is derived globally on a daily basis at 1-km spatial resolution and composited over eight-day time intervals.

We also used an alternative MOD17A2 product developed using daily surface meteorological inputs from the National Centers for Environmental Prediction–National Center for Atmospheric Research (NCEP–NCAR) reanalysis (NNR) [6].

The MOD17-NNR and MOD17-GMAO products differ in that the NNR surface air temperature, solar radiation, and VPD data have been corrected for regional bias using daily observations from the pan-boreal regional surface weather station network. Both MODIS data sets are used in this investigation to assess TCF model sensitivity to alternative GPP inputs.

The MODIS GPP inputs are derived globally at 1-km spatial resolution and eight-day intervals. The eight-day 1-km MODIS FPAR/LAI data used for these calculations are screened to remove cloud contamination and snow effects indicated by the daily MOD15A2 QC fields [52]. The GPP data were resampled to a daily time step by temporal linear interpolation of adjacent eight-day values. The GPP values were then aggregated to a 25-km spatial resolution by averaging values of the dominant land-cover class indicated by the MODIS 1-km-resolution global land-cover classification within each 25-km grid cell. The data were then reprojected to a 25-km polar EASE grid centered over each study site location using a nearest neighbor resampling scheme.

2) SM and Temperature: Daily soil temperature inputs were derived using multifrequency dual-polarized Level-2A (L2A) brightness temperatures (T_b)'s from AMSR-E [57], [20]. The AMSR-E sensor measures brightness temperatures at 6.9-, 10.7-, 18.7-, 23.8-, 36.5-, and 89-GHz frequencies. The native resolution of each frequency ranges from approximately 5 km $\times$ 5 km at 89 GHz to 60 km $\times$ 60 km at 6.9 GHz. The L2A data represent T_b from all frequencies resampled to the 6.9-GHz 60-km $\times$ 60-km native resolution [57]. The Aqua satellite is polar-orbiting with 1-A.M./P.M. equatorial crossing times, providing multiple daily acquisitions in polar regions [58]. For high-latitude regions, the overlapping orbital swaths allow two to four T_b observations per footprint overpass with a typical standard deviation of approximately 1 K ($\max = 5$ K) at 6.9 GHz and < 1 K ($\max = 3.5$ K) at 89 GHz. The T_b observations were extracted from Level-2A orbital swath footprints whose centroid falls within 5 km of each site location. Therefore, the observations can be considered to be representative of an approximate 60-km $\times$ 60-km pixel centered over each location. The descending (A.M.) overpass of Aqua occurs between 3- and 6-A.M. local time within the study domain. The T_b observation with the earliest overpass time was selected to represent the time-of-day when the soil profile is closest to isothermal conditions. Low-frequency ($\leq$10.7-GHz) T_b values may be contaminated by radio-frequency interference (RFI) typically associated with metropolitan areas [59]; however, the influence of RFI was not observed at the study locations and is not considered to be a significant factor in sparsely populated boreal–Arctic regions [20]. Daily soil temperatures were derived using an empirical approach developed over the study sites using AMSR-E daily multifrequency T_b values with separate coefficients for frozen and nonfrozen conditions. This approach yielded respective accuracies of 2.82 and 4.68 K [root-mean-square error (rmse)] under nonfrozen and frozen conditions relative to site-based measurements [20].

Daily SM inputs were obtained from the AMSR-E Level-3 (L3) operational SM product projected to a 25-km-resolution global EASE grid [60]. The L3 SM product is based on a change-detection algorithm with dual-polarized low-frequency daily T_b observations and a simplified radiative transfer equation for vegetation-covered soil [61]. Although the 6.9-GHz frequency has greater potential SM sensitivity, the 10.7-GHz frequency was used in the L3 algorithm to mitigate RFI in the 6.9-GHz band over populated areas [59]. The monthly minimum of the normalized T_b polarization difference ratio [e.g., $(T_{\rm bv} - T_{\rm bh})/(T_{\rm bv} + T_{\rm bh})$] at 10.7 GHz linearly interpolated between months provides a daily lumped vegetation roughness factor and also defines dry soil conditions [61]. The vegetation roughness factor is included in an exponential term that amplifies the change in daily polarization ratio observations above dry soil baseline conditions. The algorithm does not explicitly account for open-water (WAT) effects, but the use of the monthly minimum polarization ratio for determining a baseline reduces its influence.

The L3 product has relative merits for boreal and tundra landscapes over other satellite-based SM products because it partially accounts for WAT effects. However, a limited dynamic range of the L3 product has been reported in regional validation studies [62], although the total information content of the retrievals was found to be similar to other AMSR-E-based SM algorithms for the continental U.S. [63]. We therefore scaled the NASA L3 product between maximum and minimum values for the three-year observation period at each site location to produce an index of relative wetness varying between 0% and 100%. Under frozen conditions, the $W_{\rm mult}$ parameter in (8) was set to unity, and soil temperature was used as the sole constraint on TCF soil respiration rate calculations. The relative accuracy (rmse) of the L3 SM product has been estimated to be $\pm$12.8% of saturation under conditions where the overlying vegetation water content is less than 1.5 kg/m^{-2} [18]. Relative accuracy in AMSR-E-derived SM was reported as $\pm$29.4% of saturation over continental vegetation in Spain [62]. Comparisons with station observations and site-based model simulations at the boreal–Arctic study sites indicate an L3 product accuracy (rmse) from 15% to 41% of saturation for site windows composed of $\leq$ 25% WAT and peak annual LAI $\leq$ 4, with much of the error being due to bias from limited temporal variability [64].

D. Model Assessment

Model simulations were compared with tower-CO_2-eddy-covariance-measurement-derived carbon fluxes and terrestrial ecosystem process model simulations across the regional station network to verify model consistency with the other methods in terms of representing cross-site spatial patterns and daily-to-annual variability in NEE and component carbon fluxes. The dominant vegetation class of the overlying TCF grid cells was generally consistent with the more spatially constrained ($\sim$1-km) tower footprints except for the OAS site where the TCF grid cell included cropland (CRP) and MXF rather than the mature deciduous forest of the tower footprint. The TCF simulations were also compared with BIOME-BGC ecosystem process model simulations of daily and annual carbon fluxes at all study sites. The BIOME-BGC simulations were conducted using similar regional land-cover class and daily meteorological inputs as the TCF simulations and

associated MOD17A2 GPP inputs. The MOD17A2 results have previously been compared with site-derived GPP (e.g., [53]); these results indicate that the MODIS GPP inputs are generally larger but within 20%–30% of tower-based fluxes.

TCF model results were evaluated with respect to terrestrial carbon fluxes from alternate ecosystem process model and stand-level CO_2 eddy covariance measurement approaches in terms of producing similar magnitudes, spatial patterns, and daily and annual variability in carbon fluxes while recognizing that all of these methods are imperfect and incorporate various degrees of uncertainty. Model accuracy was assessed using least squares linear regression analysis of independent (TCF) and dependent variables. Validation statistics describing TCF model error relative to the other methods included coefficient of determination (R^2), rmse, and mean residual (MR) error terms. A sensitivity analysis was conducted to assess TCF model responses to alternate GPP inputs and uncertainty in AMSR-E SM and temperature inputs.

1) Comparisons With Tower CO_2 Flux Measurement Approaches: TCF model results were compared with tower-eddy-covariance-measurement-derived estimates of daily NEE, GPP, and ecosystem respiration $(R_{\rm tot})$ from 2002 to 2004 for the BRO, ATQ, IVO, LTH, OBS, and OAS sites, where $R_{\rm tot}$ is defined as the sum of R_a and R_h. Daily flux data for the BRO_2, LTH, OAS, and OBS sites represent gap-filled and friction-velocity-filtered records derived from integrated half-hourly CO_2 flux measurements that include calculated GPP and $R_{\rm tot}$ terms, where gap-filling procedures included either mean diurnal variation, nonlinear regression, or seasonal lookup table approaches [65], [66]. Gap-filled daily NEE data for the BRO_1, ATQ, and IVO sites were derived by first modeling $R_{\rm tot}$ and GPP (see hereafter) and then computing NEE as a residual difference. Half-hourly $R_{\rm tot}$ for the tundra sites was calculated using the Eyring function, which is based on soil temperature [67], [68]. When NEE data were available, half-hourly GPP was calculated as the difference between the modeled $R_{\rm tot}$ and observed NEE. When NEE was missing or of poor quality, GPP was calculated using measured photosynthetically active radiation and a Michaelis–Menton rate response curve. Parameters for the response functions were derived from observed NEE and micrometeorological data [67], [68].

2) Comparisons With Ecosystem Process Model Simulations: We used version 4.2 of the BIOME-BGC model to simulate daily NEE and component carbon fluxes for each of the study sites. The BIOME-BGC ecosystem process model is designed to simulate fluxes and storage of carbon, water, and nitrogen for terrestrial biomes ranging from individual plot to global scales. The model has been successfully applied over a range of diverse biomes, spatial scales, and climate regimes including boreal forest and tundra landscapes of Alaska and Canada [51], [69]–[73]. Details of the model are presented elsewhere and include applications for multiple biome types and spatial scales (e.g., [74] and [75]), while a summary of model components pertaining to this investigation is provided hereafter.

The BIOME-BGC model is designed to realistically simulate soil–plant carbon (C) and nitrogen (N) cycling but with simplifying assumptions to facilitate application at regional scales using a limited number (34) of biome-specific physiological constants. All plant, litter, and soil carbon; nitrogen; and water pools and fluxes are entirely prognostic. The plant/ecosystem surface is represented by single, homogenous canopy, snow (when present), and soil layers, where understory vegetation is not distinguished from the aggregate canopy layer. The model operates on a daily time step, with daily maximum and minimum air temperatures, incident solar shortwave (direct and diffuse) radiation, and precipitation as primary inputs from which mean daily net radiation, VPD, and day/night average temperatures are estimated. Biophysical processes represented by the model include photosynthetic C fixation from atmospheric CO_2; N uptake from the atmosphere and soil; C/N allocation to growing plant parts; seasonal phenology and decomposition of fresh plant litter and soil organic matter; plant mortality, growth, litterfall, decomposition, and disturbance (i.e., fire and management); solar radiation interception and partitioning into sunlit and shaded leaf fractions; rainfall routing to leaves and soil; snow accumulation and melting; drainage and runoff of soil water; evaporation of water from soil and wet leaves; and ET partitioning into transpiration, snow, soil, and canopy evaporation components.

NPP is determined as the daily difference between GPP and autotrophic respiration (R_a) from maintenance (R_m) and growth (R_g) processes. Photosynthesis, including both C_3 and C_4 pathways, is calculated separately for sunlit and shaded canopy components using a modified form of the Farquhar biochemical model [76]. Photosynthetic response is regulated by canopy conductance to CO_2, leaf maintenance respiration, and daily meteorological conditions including air pressure, air temperature, and solar irradiance. Canopy CO_2 conductance is calculated as a proportion of the canopy conductance to water vapor (g_c), which is derived from a prescribed maximum rate modulated for suboptimal air temperature, VPD, solar irradiance, or soil water potential conditions [75], [77]. The R_m term represents the total C losses from day and night foliar, sapwood, and coarse- and fine-root respiration components of living tissue. R_m is calculated from a base respiration rate adjusted for tissue N concentration and an empirical exponential relationship to estimated daily air and soil temperatures [78]. The R_g term is calculated as a constant proportion of new tissue carbon construction for woody and nonwoody tissue types.

NEE is calculated on a daily basis as the difference between NPP and soil heterotrophic respiration (R_h). The R_h term is estimated as a daily rate defined from soil and litter C pools. Soil and litter decomposition and R_h are defined as the aggregate result of characteristic exponential decay functions for a series of seven cascading litter and soil C pools of decreasing substrate quality. Daily R_h within each C pool is calculated from an empirical decomposition rate modulated by daily soil water potential, soil temperature, and soil N conditions.

Relative proportions of C and N within soil, litter, and vegetation compartments are tightly coupled; plant growth and allocation, soil decomposition, respiration and N mineralization, and immobilization are strongly regulated by C and N availability defined from prescribed C: N ratios for individual compartments and environmental conditions. Vegetation canopy and fine-root phenology determines the seasonal pattern

TABLE III
COMPARISON OF TCF-MODEL-BASED SURFACE ($\leq$ 10-cm DEPTH) SOC (IN GRAMS OF CARBON PER SQUARE METER) RELATIVE TO ALTERNATIVE ESTIMATES FROM BIOME-BGC (BGC) SITE SIMULATIONS, GLOBAL SOIL CARBON INVENTORY, AND SITE MEASUREMENT RESULTS

Site	C_{met}	C_{str}	C_{rec}	TCF[a]	BGC[c]	IGBP-DIS[b,c]	Site[c]	L[d]
BRO	11	28	3220	3259	3107	1889	1900-4700	1
ATQ	93	26	2790	2909	2462	1889	3800	2
UPD	149	29	4900	5078	3909	1889	2700-4400	1
HPV	83	33	2050	2166	4524	2529	1800	1
IVO	94	31	2630	2755	5189	2529	3800-10400	3
IARC	86	117	4280	4483	2972	2794	2882-4758	6
OBS	95	129	5110	5334	2146	5324	4300	7
OAS	129	114	3930	4173	5148	3050	1943-9029	5
LTH	77	32	1190	1299	1050	1509	2902	4

[a]Total SOC computed as sum of TCF derived C_{met}, C_{str} and C_{rec} components;
[b]Global Gridded Surfaces of Selected Soil Characteristics (IGBP-DIS) data set [82];
[c]Soil carbon density values adjusted to 10cm soil depth by assuming uniform vertical distribution of SOC;
[d]Literature source of site based SOC values: 1. [84]; 2. [23]; 3. [85]; 4. [29]; 5. [86]; 6. [87]; 7. [88].

of canopy photosynthesis, growth, senescence, and dormancy and is calculated for both evergreen and deciduous vegetation from an empirical phenology model and deviations of current air temperature, SM, and incident solar radiation conditions from long-term climatology of the site [74], [79]. Atmospheric N deposition occurs at a constant daily rate directly to a soil mineral N pool; N leaching and removal from the system occurs as a constant fraction of soil water outflow. Whole-plant mortality is calculated, in addition to seasonal canopy and fine-root losses, as a prescribed annual fraction of plant biomass scaled to a daily loss rate, which is then transferred to soil litter pools. Annual fire mortality is also specified as a biome-specific physiological parameter scaled to a constant daily rate of consumption for aboveground biomass, and root and soil litter C and N pools [74].

BIOME-BGC (BGC) simulations of vegetation and soil carbon stocks were conducted for the dominant vegetation class within 25-km windows centered over each site location. Vegetation classes within each window were identified using the 1-km-resolution MODIS IGBP global land-cover classification [21]. Simulations were initialized by "spinning up" the model through continuous cycling of available (1979–2004) daily meteorological time series from local weather station records, and model assumptions of constant annual fire disturbance and mortality rates within individual biomes, constant atmospheric N deposition, and constant atmospheric CO_2 levels. Long-term daily meteorological inputs for the BGC spin-up runs were developed for each site through spatial interpolations of nearby weather station records from the National Climate Data Center's TD-3210 First Order Summary of the Day [80] using the MT-CLIM microclimate simulation model [81], [82]. A second series of BGC simulations was then conducted to estimate daily carbon fluxes over the three-year (2002–2004) study period for each site location using coincident GMAO-reanalysis-based daily solar radiation, air temperature, and humidity inputs under constant atmospheric N deposition and annual fire disturbance rates, and historical atmospheric CO_2 concentrations. Daily precipitation inputs for these model runs were obtained from local weather station records because precipitation data were not available from the GMAO reanalysis. The resulting 2002–2004 BGC simulation results were then compared with available tower-measurement-derived estimates of daily carbon fluxes and TCF results for each site location.

III. RESULTS

A. Surface SOC Stocks

The TCF simulations of surface SOC stocks are summarized in Table III. Model initializations of recalcitrant SOC stocks to steady-state conditions from continuous cycling of the three-year MODIS GPP and AMSR-E-based soil temperature and moisture series required approximately 350 and 1000 years for the boreal and tundra sites, respectively, while initialization of metabolic and structural SOC pools was generally attained within five years. The TCF-derived total SOC stocks ranged from 1299 $g \cdot C \cdot m^{-2}$ for the GRS site to approximately 4663 ($\pm$601 SD) $g \cdot C \cdot m^{-2}$ and 3233 ($\pm$1104 SD) $g \cdot C \cdot m^{-2}$ for the boreal forest and tundra sites. Model simulations of metabolic and structural carbon pools were less than 6% and 3% of the total estimated SOC pools, respectively. These results generally reflect conditions within the top 10 cm of the soil, as characterized by AMSR-E-based soil temperature and moisture inputs. The rmses of site differences between TCF simulations of surface SOC stocks and alternate-BGC- and global-soil-carbon-inventory-derived estimates were 736 and 596 $g \cdot C \cdot m^{-2}$, respectively, and represented approximately 22% of these alternate SOC stocks. The TCF- and BGC-derived results were also within the range of reported SOC values from site soil inventories.

B. Daily and Seasonal Carbon Fluxes

Daily variability and seasonal patterns of terrestrial carbon fluxes were similar between TCF and BGC simulations, and available tower-eddy-covariance-measurement-based approaches. These relationships are summarized in Table IV, while seasonal patterns of daily carbon fluxes are shown in Fig. 2 for the OBS boreal forest and BRO tundra sites. The MODIS-based GPP inputs to the TCF model accounted for more than 77% of daily variability in tower-derived GPP for the boreal forest and GRS sites, while correspondence was reduced for the less productive tundra sites with relatively sparse data records. At Barrow, the MODIS GPP results were intermediate between relatively productive BRO_2 and less productive BRO_1 tower results. Model agreement was also lower for the BRO and ATQ sites where the sample size (N) of daily tower fluxes was greatly reduced relative

TABLE IV
SUMMARY OF RELATIVE AGREEMENT IN ESTIMATED SITE DAILY CARBON FLUXES BETWEEN MODEL (TCF AND BIOME-BGC) AND AVAILABLE TOWER-CO_2-FLUX-MEASUREMENT-DERIVED RESULTS (DEPENDENT VARIABLE), WHERE BIOME-BGC RESULTS ARE IN BRACKETS

TCF [BIOME-BGC] vs Tower

		GPP (g C m^{-2} d^{-1})			R_{tot} (g C m^{-2} d^{-1})			NEE (g C m^{-2} d^{-1})		
Site	N[a]	R^2 (%)	RMSE	MR[b]	R^2 (%)	RMSE	MR[b]	R^2 (%)	RMSE	MR[b]
BRO_1	181	1.3	0.865	-0.217	30.6	0.524	-0.333	1.5	1.044	-0.121
		[13.8]	[0.621]	[0.274]	[2.1]	[0.489]	[-0.179]	[8.6]	[0.937]	[-0.458]
BRO_2	223	63.7	1.072	0.891	6.3	0.562	-0.520	27.2	1.590	-1.180
		[26.6]	[1.488]	[1.219]	[3.0]	[0.426]	[-0.183]	[2.5]	[1.859]	[-1.403]
ATQ	185/94	38.5	0.957	-0.729	40.2	0.709	-0.541	4.3	0.689	0.292
		[12.1]	[0.510]	[-0.348]	[26.8]	[0.267]	[-0.179]	[2.9]	[0.493]	[0.324]
IVO	457	53.7	0.925	-0.330	67.9	0.563	-0.219	14.4	0.569	0.071
		[59.6]	[1.261]	[-0.625]	[64.7]	[0.943]	[-0.413]	[22.4]	[0.504]	[0.172]
OBS	1095	83.0	1.042	-0.174	73.4	0.976	-0.288	48.3	0.721	-0.107
		[87.7]	[0.772]	[-0.081]	[87.9]	[0.626]	[0.062]	[50.8]	[0.714]	[0.150]
OAS	1095	77.9	1.487	-0.173	87.5	1.294	-0.819	26.3	1.958	-0.461
		[59.6]	[2.015]	[-0.298]	[86.2]	[0.762]	[-0.526]	[22.3]	[1.936]	[-0.043]
LTH	1095	80.1	1.811	0.750	69.2	0.459	-0.051	49.9	1.727	-0.742
		[68.5]	[2.049]	[0.844]	[70.6]	[0.505]	[0.130]	[45.9]	[1.752]	[-0.655]

TCF vs BIOME-BGC

		GPP (g C m^{-2} d^{-1})			R_{tot} (g C m^{-2} d^{-1})			NEE (g C m^{-2} d^{-1})		
Site	N	R^2 (%)	RMSE	MR[c]	R^2 (%)	RMSE	MR[c]	R^2 (%)	RMSE	MR[c]
BRO	1095	80.6	0.407	-0.095	72.6	0.342	-0.119	1.6	0.422	-0.024
ATQ	1095	83.1	0.342	-0.023	86.0	0.287	-0.082	6.9	0.299	-0.059
UPD	1095	72.2	0.469	0.150	57.4	0.430	0.104	29.7	0.368	-0.046
HPV	1095	80.6	0.574	0.153	84.6	0.442	0.131	26.9	0.426	-0.022
IVO	1095	84.6	0.715	0.381	84.2	0.581	0.267	30.5	0.460	-0.113
IARC	1095	90.1	1.246	0.729	94.0	0.595	0.284	53.8	1.084	-0.445
OBS	1095	84.2	1.009	-0.093	88.6	0.744	-0.350	41.1	0.803	-0.257
OAS	1095	79.2	1.224	0.125	87.2	0.969	-0.293	35.1	1.092	-0.418
LTH	1095	71.1	0.589	-0.094	78.0	0.398	-0.181	20.2	0.567	-0.087

[a]Sample size of daily carbon fluxes derived from tower flux measurements that were used to compute summary statistics; for ATQ, N=185 for NEE, while N=94 for GPP and R_{tot};

[b] $\dfrac{\sum_{i=1}^{N}(Tower_i - TCF_i)}{N}$;

[c] $\dfrac{\sum_{i=1}^{N}(BGC_i - TCF_i)}{N}$

to the other sites and largely confined to spring and summer conditions.

The accuracy of MODIS GPP inputs indicated by rmse differences with tower fluxes was approximately 1.17 ($\pm$0.35 SD) $g \cdot C \cdot m^{-2} \cdot day^{-1}$. MR differences between MODIS- and tower-derived GPP were approximately 41% ($\pm$28 SD) of rmse values and represented from 3% (OAS) to 118% (ATQ) of tower GPP fluxes in summer. These results are generally consistent with previous MODIS GPP accuracy assessments over North American regional tower flux networks [51], [53].

The TCF-derived $R_{\rm tot}$ daily time series accounted for more than 69% of daily variability in tower-based fluxes for the boreal sites and from 6% to 68% of tower-based $R_{\rm tot}$ for tundra, with rmse differences of approximately 0.73 ($\pm$0.30 SD) $g \cdot C \cdot m^{-2} \cdot day^{-1}$. The relative correspondence between TCF and tower results for NEE was lower, with TCF-derived NEE rates accounting for between 26% and 50% of daily variability in tower fluxes for the boreal sites and less than 28% of tower variability for the tundra sites. The mean rmse between TCF- and tower-derived NEE was 1.18 ($\pm$0.56 SD) $g \cdot C \cdot m^{-2} \cdot day^{-1}$. However, daily differences between TCF- and tower-based results were both positively and negatively distributed so that the cumulative model error was reduced on an annual basis. The resulting MR differences between daily TCF results and tower-derived fluxes were approximately 43% ($\pm$26 SD) of rmse values and represented from 3% (LTH) to 99% (ATQ) of summer fluxes for $R_{\rm tot}$ and from 11% (OBS) to 359% (ATQ) of summer fluxes for NEE.

The MODIS GPP and associated TCF results showed similar accuracy as the BGC model simulations relative to daily tower flux results. The BGC simulations accounted for more than 59% and 64% of daily variability in tower-based GPP and $R_{\rm tot}$ for the boreal sites, while model agreement was reduced for tundra. The rmse differences between BGC- and tower-based GPP and $R_{\rm tot}$ averaged out to 1.24 ($\pm$0.64 SD) and 0.57 ($\pm$0.22 SD) $g \cdot C \cdot m^{-2} \cdot day^{-1}$, respectively. As with the TCF results, daily differences between BGC- and tower-derived fluxes were positively and negatively distributed so that the cumulative model error was partially mitigated over the seasonal cycle, and MR differences were approximately 43% ($\pm$23 SD) of rmse values. The MR differences represented

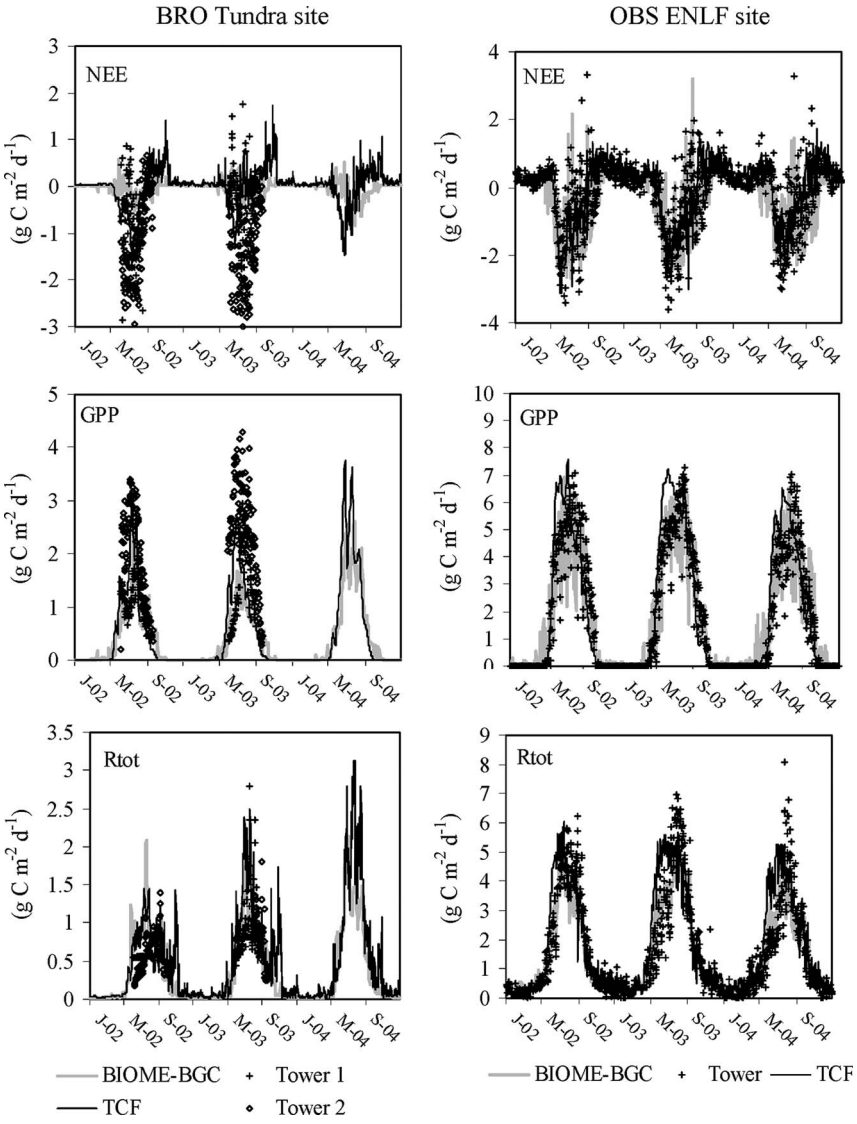

Fig. 2. Seasonal patterns of 2002–2004, daily GPP, $R_{\rm tot}$, and NEE from TCF and BIOME-BGC simulations, and tower-eddy-covariance-based CO_2 measurements for selected tundra and boreal forest [66] sites; negative and positive NEE values denote respective ecosystem uptake and loss of carbon.

from 2% (OBS) to 100% (IVO) and from 2% (OBS) to 33% (ATQ) of summer fluxes for GPP and $R_{\rm tot}$, respectively. The correspondence between BGC and tower results for NEE was also reduced, with moderate correspondence for the OBS and LTH sites ($R^2 > 45\%$), reduced correspondence for the OAS and IVO sites ($R^2 = 22\%$), and relatively low correspondence for the other tundra sites ($R^2 < 10\%$). The BGC-derived rmse for NEE averaged out to 1.17 ($\pm$0.65 SD) $\rm g \cdot C \cdot m^{-2} \cdot day^{-1}$, while MR differences were approximately 41% ($\pm$25 SD) of the rmse and represented from 1% (OAS) to 399% (ATQ) of summer fluxes.

The correspondence between TCF- and BGC-derived daily fluxes for $R_{\rm tot}$ was generally stronger than relations between either model- and tower-derived fluxes (Table IV). The correspondence between MODIS- and BGC-derived GPP results was also strong ($R^2 > 71\%$), with respective average rmse and MR differences of 0.73 ($\pm$0.35 SD) $\rm g \cdot C \cdot m^{-2} \cdot day^{-1}$ and 0.14 ($\pm$0.27 SD) $\rm g \cdot C \cdot m^{-2} \cdot day^{-1}$. TCF-based daily $R_{\rm tot}$ rates accounted for between 57.4% (UPD) and 94.0% (IARC) of daily variability in BGC results, while respective rmse differences averaged out to 0.53 ($\pm$0.22 SD) $\rm g \cdot C \cdot m^{-2} \cdot day^{-1}$. The MR differences for $R_{\rm tot}$ were approximately 37% ($\pm$9 SD) of rmse values and represented from 5% (HPV) to 13% (LTH) of BGC-derived summer fluxes. Heterotrophic respiration represented approximately 47% ($\pm$10 SD) and 55% ($\pm$2 SD) % of the annual $R_{\rm tot}$ rate for BGC and TCF results, respectively. During the summer months, TCF-derived R_h represented approximately 43% ($\pm$5 SD) of $R_{\rm tot}$ and was more consistent with BGC calculations. The larger proportion of R_h from the TCF results reflects lower R_a and corresponding $R_{\rm tot}$ rates under reduced solar illumination and associated GPP rates in winter from which R_a was derived. The primary sources of TCF-derived heterotrophic respiration were from the $C_{\rm met}$ and $C_{\rm str}$ pools, which represented approximately 66% ($\pm$10.4 SD) and 14% ($\pm$8.4 SD) of the annual R_h rate, respectively, even though these pools were less than 6% of the total SOC stocks. In contrast, $C_{\rm rec}$ contributed only 19% ($\pm$4.1 SD) of R_h but was the dominant SOC component.

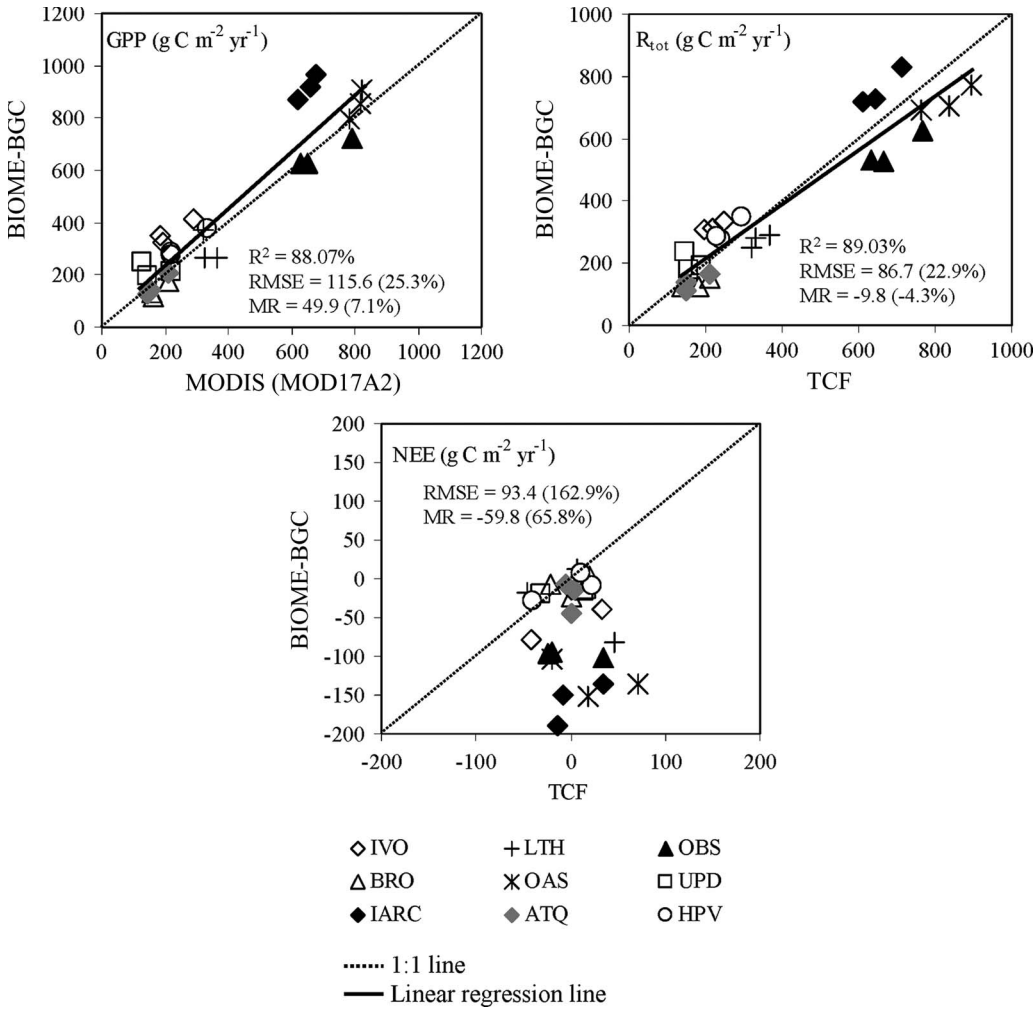

Fig. 3. Scatterplots and corresponding significant $(P < 0.05)$ linear regression results between TCF- and BIOME-BGC-derived annual carbon fluxes for the regional network of boreal forest, GRS, and tundra sites; negative and positive NEE values denote respective ecosystem uptake and loss of carbon.

As with model comparisons with tower results, agreement between daily TCF and BGC results for residual NEE fluxes was lower than for component GPP and $R_{\rm tot}$ fluxes. The TCF results accounted for between 35% (OAS) and 54% (IARC) of daily variability for the boreal forest sites and less than 31% of variability in BGC results for the GRS and tundra sites. For NEE, the rmse differences between TCF and BGC results averaged out to 0.61 ($\pm$0.30 SD) $\rm g \cdot C \cdot m^{-2} \cdot day^{-1}$, while MR values averaged out to 22% ($\pm$13 SD) of the rmse and represented from 5% (ATQ) to 28% (BRO) of summer fluxes.

C. Annual Carbon Fluxes

Relations between TCF and BGC simulations of annual GPP and $R_{\rm tot}$ fluxes were generally consistent with BGC simulations in terms of representing both site differences and annual variability of terrestrial carbon fluxes (Fig. 3). The TCF results accounted for more than 88% and 89% $(P < 0.0001)$ of BGC-based simulations of variability in annual GPP and $R_{\rm tot}$, respectively. The rmse of the estimated annual GPP between MODIS and BGC results was approximately 116 $\rm g \cdot C \cdot m^{-2} \cdot year^{-1}$ across all sites, which was approximately 25% of the BGC-derived annual flux. The errors were both positively and negatively distributed so that the MR difference for GPP was approximately 7% (50.0 $\rm g \cdot C \cdot m^{-2} \cdot year^{-1}$), while MR differences were also less than the rmse values for all other annual fluxes. For $R_{\rm tot}$, respective rmse and MR differences between TCF and BGC results were 23% (86.7 $\rm g \cdot C \cdot m^{-2} \cdot year^{-1}$) and -4.3% (9.8 $\rm g \cdot C \cdot m^{-2} \cdot year^{-1}$), while TCF-based $R_{\rm tot}$ was approximately 4% ($\pm$24) larger than the corresponding BGC results. The near-steady-state SOC conditions of the TCF simulations reflect model assumptions of dynamic equilibrium between GPP and $R_{\rm tot}$, and the near-neutral mean annual NEE rates over the three-year simulation period. In contrast, the BGC simulations show generally positive annual NEE uptake rates. The resulting rmse and MR differences for NEE were approximately 93.4 and -59.8 $\rm g \cdot C \cdot m^{-2} \cdot year^{-1}$ and represented approximately 163% and 66% of BGC annual fluxes, respectively. The relative impact of these differences was magnified relative to GPP and $R_{\rm tot}$ because of the much smaller size of the residual NEE fluxes.

A summary of site annual carbon budgets from model simulations and reported values from previous field studies is shown in Fig. 4. The MODIS-derived annual GPP results for the respective tundra, GRS, and boreal forest sites averaged out to 197, 257, and 716 $\rm g \cdot C \cdot m^{-2} \cdot year^{-1}$. The TCF-model-derived

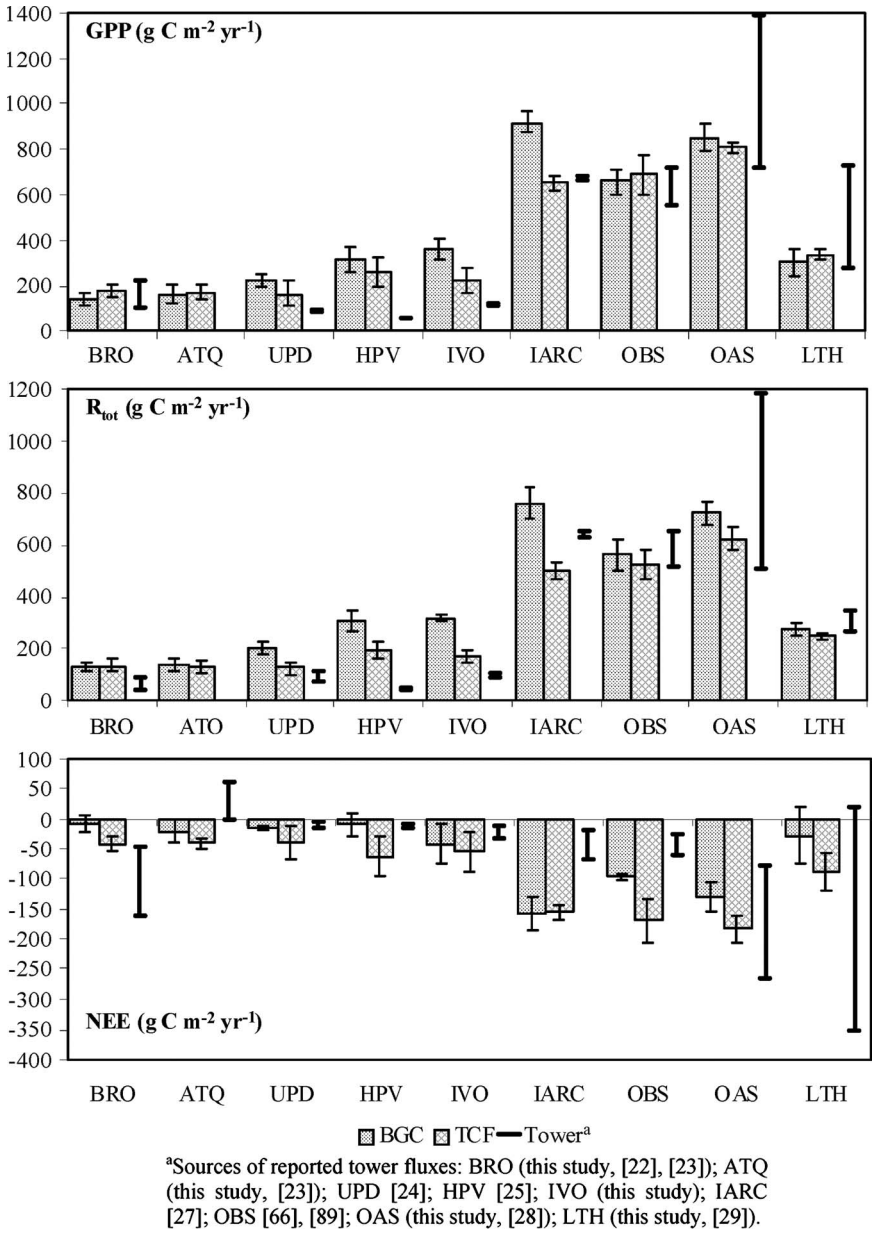

Fig. 4. Summary of site annual carbon budgets derived from BIOME-BGC (BGC) and TCF (GMAO) model simulations from this paper, and tower-based annual fluxes derived from this paper and reported values from the literature for each site; standard deviations of model-derived annual fluxes for the 2002–2004 study period are represented by thin black lines, while the range of reported tower fluxes is represented by thick black lines. The TCF GPP results are derived from the MODIS MOD17A2 (C.5) time series with GMAO climate. Site-measurement-derived fluxes for IVO, HPV, BRO, UPD and ATQ represent growing season (MJJAS or JJA) accumulations, relative to annual accumulations for the OBS, IARC, OAS, and LTH sites; for ATQ, there were insufficient tower flux data to present either seasonal or annual fluxes for GPP and R_{tot}.

R_{tot} rates averaged out to 197, 339, and 725 $\mathrm{g \cdot C \cdot m^{-2} \cdot year^{-1}}$ for the tundra, GRS, and boreal forest sites. The OAS site had the highest annual GPP and respiration fluxes, while the UPD tundra site had the lowest annual fluxes. The TCF-derived annual NEE fluxes represented model assumptions of average steady-state conditions and fluctuated within ± 72 $\mathrm{g \cdot C \cdot m^{-2} \cdot year^{-1}}$ over the three-year study period. The BIOME-BGC-based NEE fluxes indicated a predominant annual sink for atmospheric CO_2, averaging -57 (± 58) $\mathrm{g \cdot C \cdot m^{-2} \cdot year^{-1}}$ for all sites. The TCF and BGC results were generally within the range of reported annual carbon budgets from tower-based studies in terms of representing the relative magnitudes of annual fluxes and differences among the major land-cover classes. The MODIS-based GPP results were similar (i.e., within one standard deviation) to the range of reported annual rates from tower measurements for the boreal forest and GRS sites. The BGC results were also similar to tower-based annual fluxes for these sites except for IARC where the BGC results showed a larger GPP rate than either MODIS or tower results. While the MODIS- and BGC-derived GPP rates were similar for OAS and LTH, they occupied the lower range of reported tower GPP rates for these sites. For the tundra sites, there were insufficient daily tower flux data to compute annual rates, so the tower results shown in Fig. 4 reflect growing season (MJJAS or JJA) accumulations for BRO, UPD, HPV, and IVO, while daily flux measurements for ATQ were too sparse to compute reliable

cumulative fluxes for GPP or $R_{\rm tot}$. The corresponding model-based GPP rates for these sites reflect cumulative annual fluxes and were either within the upper range or more productive than the tower results.

The TCF-derived annual rates for $R_{\rm tot}$ were within the range of reported tower fluxes for the boreal forest sites. The BGC-derived $R_{\rm tot}$ rates were also similar to reported tower results for these sites except for IARC where the BGC results were larger than reported fluxes. For LTH, the BGC results were within the range of reported $R_{\rm tot}$ rates, while the TCF results were larger than both BGC- and tower-based results. For the tundra sites, the annual $R_{\rm tot}$ rates from both models were generally above the range of reported tower-based results. However, when the model results were adjusted to reflect only growing season accumulations, there was no change in GPP from annual rates, while $R_{\rm tot}$ rates were reduced by approximately 12% and were more consistent with the tundra tower results.

The TCF annual NEE results were within the range of reported values for the OBS and IARC boreal evergreen forest sites, while BGC produced larger annual carbon sinks than the tower measurements for these sites. The TCF-based NEE results were much smaller than the reported tower-based results for OAS, while the BGC results showed a much stronger net annual carbon sink for this site that was within the lower range of tower observations. Both models were within the range of tower-based NEE rates for LTH, although the tower studies indicate greater potential sink strength for this site. For the tundra sites, both models were within the range of tower-based fluxes except for the BRO site. The BGC- and TCF-derived annual NEE rates indicated near-neutral annual carbon-source–sink activity for both BRO and ATQ sites, while the corresponding tower-derived seasonal fluxes indicated a moderate net annual carbon sink and source for BRO and ATQ, respectively. Adjustment of the model results to reflect growing season accumulations for the tundra sites increased carbon sink strength by approximately 32% and was more consistent with the tower results for BRO but less similar for ATQ.

D. TCF Sensitivity to Remote Sensing Inputs

The TCF algorithm sensitivity to daily GPP inputs was assessed by evaluating the relative impact of alternative MOD17-GMAO and MOD17-NNR GPP inputs on the estimated carbon fluxes. The MOD17-NNR-based daily GPP corresponded closely with MOD17-GMAO results ($R^2 = 0.889$ and $P < 0.0001$) but was approximately 31% less than the baseline GPP inputs. The reduced productivity was primarily due to regional bias correction and associated reductions in reanalysis solar radiation inputs to the production efficiency model [6]. The use of these alternate GPP inputs resulted in average 13% ($\pm$25 SD) decreases in the estimated SOC stocks. The resulting annual carbon fluxes accounted for approximately 90% of the variance in baseline calculations of respiration components and more than 83% of the variance in NEE ($P < 0.0001$). Resultant annual carbon flux calculations, however, were reduced by approximately 31%.

On an annual basis, low soil temperature was the dominant environmental constraint on TCF heterotrophic respiration calculations across all sites, resulting in annual R_h rates that were approximately 82% ($\pm$9.9 SD) below potential conditions (i.e., no temperature effect). SM limitations were of secondary importance, with annual R_h rates being approximately 16% ($\pm$8.5 SD) below potential conditions (i.e., no moisture effect). These results are consistent with previous observation and modeling studies indicating that biological processes and the growing season for northern ecosystems are largely constrained by cold temperatures [90], [91]. During the growing season (MJJAS), low temperatures were also the dominant environmental constraint on daily R_h except for the relatively warm dry LTH GRS site, where SM had a greater relative impact than soil temperature. Low soil temperatures reduced daily R_h rates during the growing season within the respective tundra, boreal forest, and GRS sites by 82% ($\pm$11.1 SD), 60% ($\pm$14.9 SD), and 43% ($\pm$17.8 SD) from potential conditions. Suboptimal SM levels at these sites reduced daily R_h during the growing season by approximately 26% ($\pm$24.2 SD), 18% ($\pm$14.4 SD), and 51% ($\pm$23.8 SD), respectively. The net effect of both soil temperature and moisture limitations reduced R_h rates by 85% ($\pm$7.0 SD) and 78% ($\pm$10.2 SD) for respective annual and growing season conditions across all sites.

A sensitivity analysis was conducted to assess TCF model uncertainty from AMSR-E-derived soil temperature (T_s) and SM inputs. The error was assumed uncorrelated between T_s and SM inputs and uncorrelated through time. The model GPP inputs were assumed to contribute a constant representative error (1.2 $\rm g \cdot C \cdot m^{-2} \cdot day^{-1}$) to the TCF calculations, derived as the mean rmse difference between MODIS and tower GPP results in Table IV. The total uncertainty contributed to NEE calculations from this amount of GPP error is 0.65 $\rm g \cdot C \cdot m^{-2} \cdot day^{-1}$, with a 0.55-$\rm g \cdot C \cdot m^{-2} \cdot day^{-1}$ error contribution to the estimation of R_a and $R_{\rm tot}$. All other model parameters, including soil and litter carbon pools, were assumed to be error free. Representative SOC pools of 95 ($C_{\rm met}$), 129 ($C_{\rm str}$), and 5110 ($C_{\rm rec}$) $\rm g \cdot C \cdot m^{-2}$ were assigned for the sensitivity analysis (Table III), while respective larger and smaller SOC pools result in proportional increases or reductions in TCF estimation errors. Results of the sensitivity analysis are presented over a range of T_s and SM levels from 1 °C to 20 °C and 5% to 100% saturation, and for selected errors in T_s (under constant SM of 50%) and SM (under constant T_s of 20 °C). The expected errors for T_s and SM were 2 °C and 15%, respectively, based on comparisons of AMSR-E T_s and SM values to site biophysical measurements [18], [64].

Because of nonlinear dependence of R_h on T_s and SM in the model, error in estimated carbon fluxes (R_h, $R_{\rm tot}$, and NEE) is dependent on the magnitude of T_s and SM inputs (Fig. 5). Uncertainty in $R_{\rm tot}$ from error in T_s inputs increases exponentially with T_s, while uncertainty in $R_{\rm tot}$ from error in SM inputs is minimal near intermediate (50% saturation) moisture levels but increases under wetter or drier conditions. Uncertainty in T_s has the greatest impact on $R_{\rm tot}$ under intermediate SM conditions, whereas uncertainty in SM has the greatest impact on $R_{\rm tot}$ at the extreme wet and dry portions of the SM curve. Overall, GPP contributes the majority of uncertainty to TCF calculations of $R_{\rm tot}$ and NEE when respective errors in R_h are below 0.55 and 0.65 $\rm g \cdot C \cdot m^{-2} \cdot day^{-1}$.

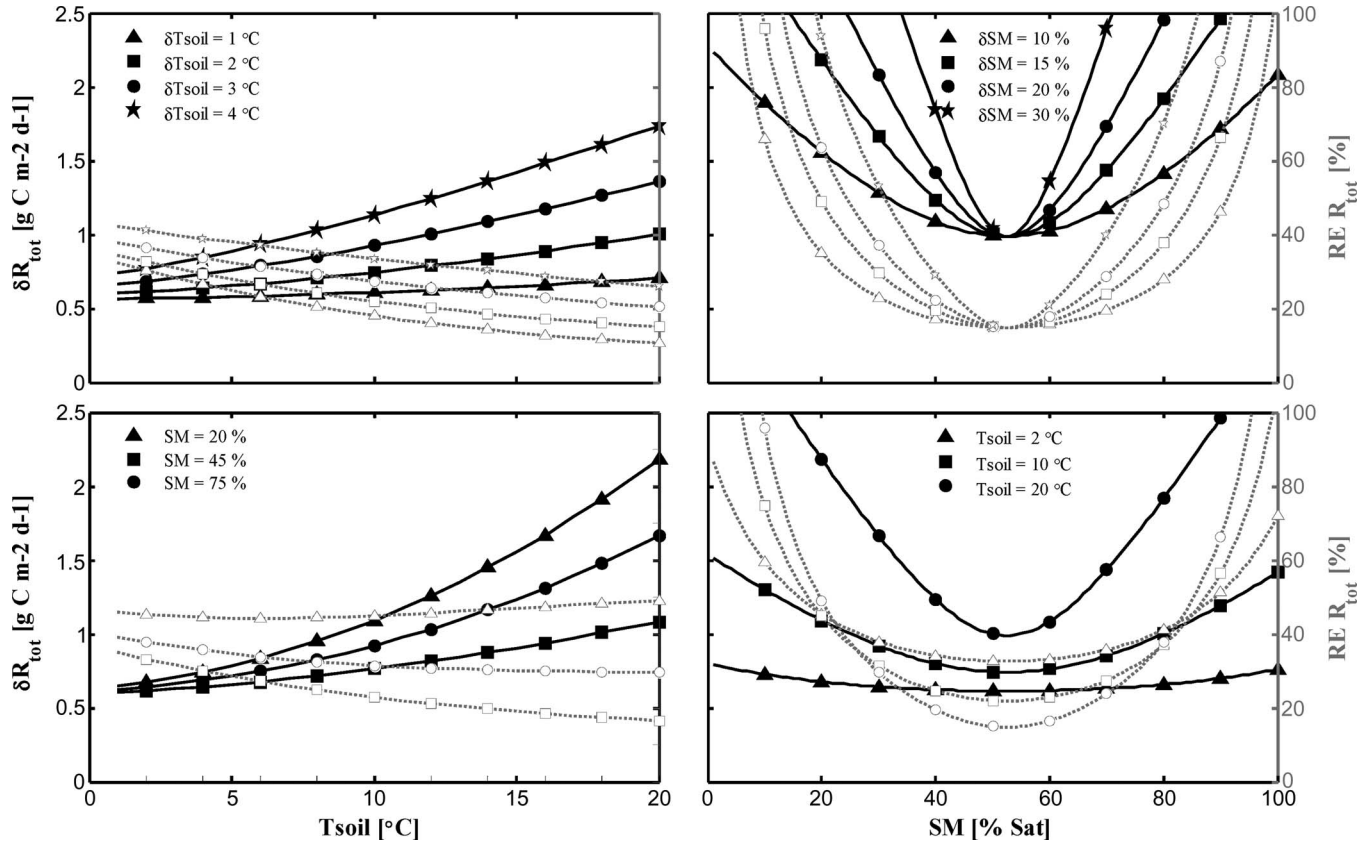

Fig. 5. Uncertainty in total ecosystem respiration ($\delta R_{\rm tot}$) from selected errors in T_s (δT_s) and SM (δSM) and a constant GPP error contribution of 1.2 g $\cdot$ C $\cdot$ m^{-2} $\cdot$ day^{-1} and constant GPP of 1.9 g $\cdot$ C $\cdot$ m^{-2} $\cdot$ day^{-1}; $\delta R_{\rm tot}$ values are shown on primary (in grams of carbon per square meter per day; left axis; black lines) and secondary (in percent, $\delta R_{\rm tot}/R_{\rm tot} \times 100$; right axis; gray lines) Y-axes under variable T_s and SM conditions (X-axis). (a) $\delta R_{\rm tot}$ under four δT_s levels and variable T_s, where SM is fixed at 50% of saturation and δSM is fixed at 15%. (b) $\delta R_{\rm tot}$ under four δSM levels and variable SM conditions, where T_s is fixed at 20 °C and δT_s is fixed at 2 °C. (c) $\delta R_{\rm tot}$ under variable T_s and three different SM levels, where δT_s is fixed at 2 °C and δSM is fixed at 15%. (d) $\delta R_{\rm tot}$ under three T_s levels and variable SM conditions, where δT_s is fixed at 2 °C and δSM is fixed at 15%.

The relative contribution of R_h error to NEE uncertainty under variable T_s and SM levels is shown in Fig. 6. Under intermediate SM conditions, uncertainty in $R_{\rm tot}$ ranges from 0.60 g $\cdot$ C $\cdot$ m^{-2} $\cdot$ day^{-1} (35%) to 1.0 g $\cdot$ C $\cdot$ m^{-2} $\cdot$ day^{-1} (15%) at $T_s = 1$ °C and 20 °C, respectively (Fig. 5). This translates to 16.5% and 69.5% of the total uncertainty in $R_{\rm tot}$, respectively, with the remaining error contribution being from GPP. For NEE, the error ranges from 0.69 to 1.05 g $\cdot$ C $\cdot$ m^{-2} $\cdot$ day^{-1}, which includes 12.5% and 62.4% from SM and T_s, respectively. Under extremely dry (10%) surface SM conditions, uncertainty in $R_{\rm tot}$ ranges from 0.69 g $\cdot$ C $\cdot$ m^{-2} $\cdot$ day^{-1} (58.7%) to 2.75 g $\cdot$ C $\cdot$ m^{-2} $\cdot$ day^{-1} (95%) at $T_s = 1$ °C and 20 °C, and uncertainties in $R_{\rm tot}$ imparted by both SM and T_s are 36% and 96%, respectively. For NEE, the error ranges from 0.77 to 2.77 g $\cdot$ C $\cdot$ m^{-2} $\cdot$ day^{-1}, while uncertainties in NEE imparted by SM and T_s are 29% and 94%, respectively.

Acceptable error levels in T_s and SM are dependent on GPP for deriving meaningful (defined as relative error $< 100\%$) $R_{\rm tot}$ information, which also depends on the relative contribution of R_h to $R_{\rm tot}$. For GPP $= 0$, meaningful $R_{\rm tot}$ values can be determined when $T_s \geq 4$ °C and error in $T_s \leq 4$ °C at intermediate SM levels. For GPP $= 0.64$ g $\cdot$ C $\cdot$ m^{-2} $\cdot$ day^{-1} and SM between 35% and 70%, meaningful $R_{\rm tot}$ values can be determined under optimal T_s (20 °C) with $\leq$30% error in SM. When GPP exceeds 7.1 g $\cdot$ C $\cdot$ m^{-2} $\cdot$ day^{-1}, meaningful $R_{\rm tot}$ values can be determined when error in $T_s \leq 3$ °C and error in SM $\leq 20\%$ across the entire range of T_s and SM conditions.

For the expected error levels ($T_s = 2$ °C and SM $= 15\%$), meaningful $R_{\rm tot}$ can be determined for all values of T_s and SM when GPP exceeds 4.4 g $\cdot$ C $\cdot$ m^{-2} $\cdot$ day^{-1}. When GPP $= 0$, meaningful $R_{\rm tot}$ values can be determined when $T_s \geq 2$ °C under optimal SM levels, and under optimal T_s conditions when SM is between 14% and 91%. Uncertainty in $R_{\rm tot}$ ranges from 0.60 to 3.05 g $\cdot$ C $\cdot$ m^{-2} $\cdot$ day^{-1}, and uncertainty in NEE ranges from 0.69 to 3.07 g $\cdot$ C $\cdot$ m^{-2} $\cdot$ day^{-1} for all T_s and SM conditions. This translates into uncertainties in annual fluxes from 6.0 to 30.5 g $\cdot$ C $\cdot$ m^{-2} for $R_{\rm tot}$ (0.7%–30% of annual flux shown in Fig. 4) and from 6.9 to 30.7 g $\cdot$ C $\cdot$ m^{-2} for NEE over a 100-day growing season.

The results of the sensitivity analysis define potential uncertainty in the model-derived carbon fluxes due to error in AMSR-E soil inputs. Overall, GPP inputs to the TCF model contribute most of the estimation error for $R_{\rm tot}$ and NEE when uncertainty in $R_{\rm h}$ is relatively small (< 0.64 g $\cdot$ C $\cdot$ m^{-2} $\cdot$ day^{-1}), which generally occurs when either T_s is low (< 10 °C) or SM is near intermediate levels. The model sensitivity to T_s uncertainty increases under drier or wetter SM levels, particularly when T_s uncertainty is high. These results indicate that the accuracy of AMSR-E soil information is sufficient to determine meaningful flux estimates over a broad

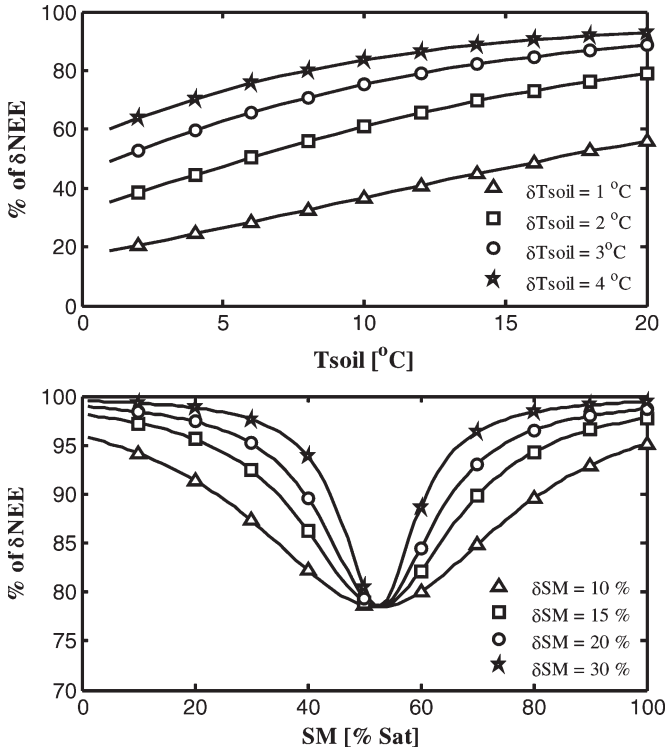

Fig. 6. Plots of the relative (in percent) contribution of both δT_s and δSM (i.e., R_h uncertainty) to TCF-derived NEE uncertainty (δNEE) under variable T_s and SM conditions. The relative contribution of GPP uncertainty is 100% minus the contributions from δT_s and δSM. (a) Relative contribution of component R_h estimation uncertainty to δNEE (Y-axis) for selected δT_s levels from 1 °C to 4 °C and variable T_s conditions (X-axis), where SM $= 50\%$ and δSM is fixed at 15%. (b) Relative contribution of component R_h estimation uncertainty to δNEE for selected δSM levels from 10% to 30% and variable SM conditions (X-axis), where $T_s = 20$ °C and δT_s is fixed at 2 °C.

range of T_s and SM conditions, including the boreal forest, GRS, and tundra sites represented in this paper. These results also specify an expected level of model error due to uncertainty in surface meteorological inputs between AMSR-E and biophysical station network measurements. The actual model error may be larger or smaller, depending on correlations between model inputs, model or measurement bias, and potential error in model representation of biophysical processes. In general, rmse values for the estimated carbon fluxes from this paper are consistent with the results of the sensitivity analysis under the prevailing climatic conditions of the study site locations.

IV. Discussion and Conclusion

The TCF and BGC model simulations from this paper show similar accuracy with respect to tower-CO_2-eddy-covariance-based estimates of NEE and component carbon fluxes. The TCF-derived fluxes showed respective rmse values of 1.2, 0.7, and 1.2 $\mathrm{g \cdot C \cdot m^{-2} \cdot day^{-1}}$ for GPP, R_{tot}, and NEE fluxes, while MR differences were approximately 43% of the rmse. The BGC simulations also produced rmse values between 0.6 and 1.2 $\mathrm{g \cdot C \cdot m^{-2} \cdot day^{-1}}$ and MR differences that were approximately 42% of the rmse.

The correspondence between TCF and BGC results was generally better than either model's agreement with tower-derived carbon fluxes. The TCF results reproduced annual variability and site differences in BGC-derived GPP and R_{tot} fluxes to within 26% and 8% accuracies relative to respective rmse and MR terms. However, the TCF results did not correspond significantly ($P > 0.05$) with BGC simulations of annual NEE. The rmse between model results was approximately 93 $\mathrm{g \cdot C \cdot m^{-2} \cdot year^{-1}}$ (163%), which was large, given the small size of the residual NEE fluxes. Thus, while the TCF model is generally consistent with more detailed ecosystem process model simulations for GPP and respiration fluxes, model results diverge for smaller residual NEE fluxes. A major cause of model NEE divergence is that the TCF simulations represent steady-state SOC conditions and associated dynamic equilibrium between GPP and R_{tot}. In contrast, the BGC simulations indicate a predominant sink for atmospheric CO_2 for most sites, which reflects disequilibrium between GPP and soil decomposition and respiration processes under rising atmospheric CO_2 levels.

The TCF-based R_{h} results represented approximately 43% and 55% of R_{tot} for respective summer and annual fluxes; these results are similar to radiocarbon analyses of temperate deciduous and boreal evergreen coniferous forests indicating that 41%–63% of soil CO_2 emissions are derived from R_h [92], [93]. The dominant source of TCF-derived R_h was from C_{met} and C_{str} stocks with a relatively high turnover rate, even though these components represented less than 6% of the total estimated SOC. These results are also consistent with radiocarbon analyses of temperate and boreal forest soils indicating that most of the CO_2 flux from soil decomposition is derived from SOC in surface ($<$ 15-cm depth) soil layers with a mean residence time of a decade or less [92], [94], which is well within the time span of current global operational satellite remote sensing records. These stocks contribute a majority of the decomposition flux but represent a relatively small component of the total SOC pool. These younger SOC stocks and associated R_h rates are also closely tied to GPP and associated photosynthate supply under steady-state conditions, as has been observed across a broad range of global biomes [94], although disturbance from fire, insect defoliations, land-use and land-cover changes, and climate perturbations may cause short-term departures from these relationships [96], [97].

There are several potential sources of differences between tower-site- and model-derived estimates of land–atmosphere carbon exchange. For this investigation, tower eddy covariance CO_2 flux measurements and associated site-based carbon flux estimates were used as ground truth for TCF and BGC simulations of carbon exchange within regional (25-km resolution) modeling windows surrounding individual tower sites. However, large uncertainties exist regarding tower measurements and their consistency with regional land–atmosphere carbon fluxes over heterogeneous landscapes. Tower GPP is calculated as the difference between NEE and R_{tot}. Estimates of R_{tot} at flux tower sites are typically made using nighttime fluxes of NEE (when photosynthesis is assumed to be zero). However, eddy flux towers can underestimate carbon fluxes by 10%–20% or more, particularly under nighttime conditions. This underestimation is fairly consistent and arises from both systematic and random errors [98]–[100] that propagate into associated GPP, R_{tot}, and NEE estimates. Bias is generally attenuated when annual NEE is considered, but has been estimated to

range from 4%–8% for temperate and boreal forests to 26% for northern agroecosystems [101]. Adverse environmental conditions, low NEE, and associated low productivity levels characteristic of tundra sites also increase sampling error and difficulty in acquiring accurate fluxes [22], [23], [102]. In addition, tower fluxes represent footprints of approximately 1 km or less and are much smaller subsamples of overlying MODIS and AMSR-E grid cells representing environmental conditions and aggregate response of the regional landscape [20], [50], [53]. Nevertheless, tower CO_2 eddy flux measurements remain a useful standard for the evaluation of surrogate measurements from satellite remote sensing, particularly when compared across regional networks spanning broad environmental and vegetation biomass gradients [9], [11], [100].

Differences between TCF and tower fluxes may also reflect the limitations of a relatively simple remote sensing algorithm to sufficiently characterize all the major processes regulating CO_2 exchange. For example, soil decomposition studies indicate that the carbon assimilation efficiency of soil microbes and associated SOC decomposition rates vary with changes in soil nitrogen availability [103] and may not be adequately represented by a constant maximum soil decomposition rate (K_{mx}). Tower-based studies at the LTH GRS site documented large increases in vegetation photosynthetic light-use efficiencies and GPP during years with increased summer precipitation and SM [29]. At the OBS forest site, automated sampling and isotopic analysis of soil respiration indicate that R_h from deep ($>$ 20-cm depth) soil layers increases with soil warming, with a significant respiration contribution being from older (centuries before present) SOC sources [104]. These processes may not be well represented by regional GPP measures and limited (three-year) sampling of near-surface soil temperature and moisture conditions from regional remote sensing measurements.

Previous studies have shown that surface soil temperature and moisture information can be retrieved with reasonable accuracy over heterogeneous landscapes from relatively coarse-resolution AMSR-E time series [18], [20]. The results of this paper indicate that AMSR-E-derived soil wetness and temperature information are effective surrogates for the primary environmental controls on soil decomposition and R_h across a broad range of boreal forest, GRS, and tundra sites. Our results also show that the integration of this information with operational-satellite-derived GPP and a simple biophysical response model provides meaningful measures of surface SOC, daily NEE, and component carbon fluxes over broad boreal–Arctic landscapes that are similar to alternative measures derived from more detailed ecosystem process model and tower eddy covariance measurement approaches. The TCF model provides an effective means for satellite-based monitoring of land–atmosphere carbon fluxes across the pan-Arctic domain, bridging the divide between relatively fine-scale CO_2 flux measurements and coarse-scale assessments of atmospheric CO_2 concentrations from sparse sampling networks and atmospheric transport models. Major assumptions of the TCF model framework are that spatial and temporal variabilities in the relative magnitude and sign of land–atmosphere CO_2 exchange are largely driven by surface soil wetness and temperature variations through direct environmental controls on R_h and that surface SOC stocks are in relative equilibrium with these environmental conditions and GPP. Further research is needed to determine how these relationships may vary over longer time periods, following disturbance, and under a warming climate.

ACKNOWLEDGMENT

The authors would like to thank the principal investigators and research teams of Ameriflux, BERMS, and FLUXNET Canada for providing the tower CO_2 flux and associated meteorological data for use in this paper. The provision of tower site measurements was provided through funding from a variety of sources including the U.S. Department of Energy Terrestrial Carbon and NASA Terrestrial Ecology programs; tower site principal investigators include S. Wofsy and A. Dunn (OBS site), T. A. Black and A. Barr (OAS site), L. Flanagan (LTH site), and Y. Harazono of the National Institute for Agro-Environmental Sciences, Tsukuba, Japan (BRO_2 site). The authors would also like to thank A. Appling for the technical assistance. Portions of the research described in this paper were carried out at the Jet Propulsion Laboratory, California Institute of Technology, Pasadena, under contract to the National Aeronautics and Space Administration.

REFERENCES

[1] J. I. House, I. C. Prentice, N. Ramankutty, R. A. Houghton, and M. Heimann, "Reconciling apparent inconsistencies in estimates of terrestrial CO_2 sources and sinks," *Tellus*, vol. 55, no. 2, pp. 345–363, Apr. 2003.

[2] C. Tarnocai, J. Kimble, and G. Broll, "Determining carbon stocks in Cryosols using the northern and mid latitudes soil database," in *Permafrost*, M. Phillips, S. Springman, and L. U. Arenson, Eds. Lisse, The Netherlands: Swets and Zeitlinger, 2003, pp. 1129–1134.

[3] W. L. Chapman and J. E. Walsh, "Recent variations of sea ice and air temperature in high latitudes," *Bull. Amer. Meteorol. Soc.*, vol. 74, no. 1, pp. 33–47, 1993.

[4] W. C. Oechel, G. L. Vourlitis, S. J. Hastings, R. C. Zulueta, L. Hinzman, and D. Kane, "Acclimation of ecosystem CO_2 exchange in the Alaskan Arctic in response to decadal climate warming," *Nature*, vol. 406, pp. 978–981, Aug. 2000.

[5] M. C. Serreze, J. E. Walsh, F. S. Chapin, III, T. Osterkamp, M. Dyurgerov, V. Romanovsky, W. C. Oechel, J. Morison, T. Zhang, and R. G. Barry, "Observational evidence of recent change in the northern high-latitude environment," *Clim. Change*, vol. 46, no. 1/2, pp. 159–207, Jul. 2000.

[6] K. Zhang, J. S. Kimball, K. C. McDonald, J. J. Cassano, and S. W. Running, "Impacts of large-scale oscillations on pan-Arctic terrestrial net primary production," *Geophys. Res. Lett.*, vol. 34, no. 21, p. L21 403, Nov. 2007. DOI: 10.1029/2007GL031605.

[7] A. Angert, S. Biraud, C. Bonfils, C. C. Henning, W. Buermann, J. Pinzon, C. J. Tucker, and I. Fung, "Drier summers cancel out the CO_2 uptake enhancement induced by warmer springs," *Proc. Natl. Acad. Sci. U.S.A.*, vol. 102, no. 31, pp. 10 823–10 827, Aug. 2005.

[8] S. Piao, P. Ciais, P. Friedlingstein, P. Peylin, M. Reichstein, S. Luyssaert, H. Margolis, J. Fang, A. Barr, A. Chen, A. Grelle, D. Y. Hollinger, T. Laurila, A. Lindroth, A. D. Richardson, and T. Vesala, "Net carbon dioxide losses of northern ecosystems in response to autumn warming," *Nature*, vol. 451, no. 7174, pp. 49–52, Jan. 2007. DOI: 10.1038/nature06444.

[9] D. Baldocchi, E. Falge, L. Gu, R. Olson, D. Holinger, S. Running *et al.*, "FLUXNET: A new tool to study the temporal and spatial variability of ecosystem-scale carbon dioxide, water vapor, and energy flux densities," *Bull. Amer. Meteorol. Soc.*, vol. 82, no. 11, pp. 2415–2434, Nov. 2001.

[10] R. Dargaville, A. D. McGuire, and P. Rayner, "Estimates of large-scale fluxes in high latitudes from terrestrial biosphere models and an inversion of atmospheric CO_2 measurements," *Clim. Change*, vol. 55, no. 1/2, pp. 273–285, Oct. 2002.

[11] S. W. Running, D. D. Baldocchi, D. P. Turner, S. T. Gower, P. S. Bakwin, and K. A. Hibbard, "A global terrestrial monitoring network integrating tower fluxes, flask sampling, ecosystem modeling and EOS satellite data," *Remote Sens. Environ.*, vol. 70, no. 1, pp. 108–127, Oct. 1999.

[12] S. W. Running, R. R. Nemani, F.-A. Heinsch, M. Zhao, M. Reeves, and H. Hashimoto, "A continuous satellite-derived measure of global terrestrial primary production," *BioScience*, vol. 54, no. 6, pp. 547–560, Jun. 2004.

[13] A. S. Hope, J. B. Fleming, G. Vourlitis, D. A. Stow, W. C. Oechel, and T. Hack, "Relating CO_2 fluxes to spectral vegetation indices in tundra landscapes: Importance of footprint definition," *Polar Rec.*, vol. 31, no. 177, pp. 245–250, 1995.

[14] C. E. McMichael, A. S. Hope, D. A. Stow, J. B. Fleming, G. Vourlitis, and W. Oechel, "Estimating CO_2 exchange at two sites in Arctic tundra ecosystems during the growing season using a spectral vegetation index," *Int. J. Remote Sens.*, vol. 20, no. 4, pp. 683–698, Mar. 1999.

[15] G. L. Vourlitis, W. C. Oechel, A. Hope, D. Stow, B. Boynton, J. Verfaillie, Jr., R. Zulueta, and S. J. Hastings, "Physiological models for scaling plot measurements of CO_2 flux across an Arctic tundra landscape," *Ecol. Appl.*, vol. 10, no. 1, pp. 60–72, Feb. 2000.

[16] C. Potter, S. Klooster, R. Myneni, V. Genovese, P.-N. Tan, and V. Kumar, "Continental-scale comparisons of terrestrial carbon sinks estimated from satellite data and ecosystem modeling 1982–1998," *Glob. Planet. Change*, vol. 39, no. 3/4, pp. 201–213, Nov. 2003.

[17] T. J. Jackson, D. M. Le Vine, A. Y. Hsu, A. Oldak, P. J. Starks, C. T. Swift, J. D. Isham, and M. Haken, "Soil moisture mapping at regional scales using microwave radiometry: The Southern Great Plains Hydrology Experiment," *IEEE Trans Geosci. Remote Sens.*, vol. 37, no. 5, pp. 2136–2151, Sep. 1999.

[18] E. G. Njoku, T. J. Jackson, V. Lakshmi, T. K. Chan, and S. V. Nghiem, "Soil moisture retrieval from AMSR-E," *IEEE Trans Geosci. Remote Sens.*, vol. 41, no. 2, pp. 215–229, Feb. 2003.

[19] Fily, M. A. Royer, K. Goita, and C. Prigent, "A simple retrieval method for land surface temperature and fraction of water surface determination from satellite microwave brightness temperatures in sub-Arctic areas," *Remote Sens. Environ.*, vol. 83, no. 3, pp. 328–338, 2003.

[20] L. A. Jones, J. S. Kimball, K. C. McDonald, S. K. Chan, E. G. Njoku, and W. C. Oechel, "Satellite microwave remote sensing of boreal and Arctic soil temperatures from AMSR-E," *IEEE Trans. Geosci. Remote Sens.*, vol. 45, no. 7, pp. 2004–2018, Jul. 2007.

[21] M. A. Friedl, D. K. McIver, J. C. F. Hodges *et al.*, "Global land cover mapping from MODIS: Algorithms and early results," *Remote Sens. Environ.*, vol. 83, no. 1/2, pp. 287–302, Nov. 2002.

[22] Y. Harazono, M. Mano, A. Miyata, R. C. Zulueta, and W. C. Oechel, "Inter-annual carbon dioxide uptake of a wet sedge tundra ecosystem in the Arctic," *Tellus*, vol. 55, no. 2, pp. 215–231, Apr. 2003.

[23] H.-J. Kwon, W. C. Oechel, R. C. Zulueta, and S. J. Hastings, "Effects of climate variability on carbon sequestration among adjacent wet sedge tundra and moist tussock tundra ecosystems," *J. Geophys. Res.*, vol. 111, no. G3, p. G03 014, Sep. 2006. DOI: 10.1029/2005JG000036.

[24] W. C. Oechel, G. L. Vourlitis, S. J. Hastings, R. P. Ault, Jr., and P. Bryant, "The effects of water table manipulation and elevated temperature on the net CO_2 flux of wet sedge tundra ecosystems," *Glob. Change Biol.*, vol. 4, pp. 77–90, 1998.

[25] G. L. Vourlitis and W. C. Oechel, "Eddy covariance measurements of CO_2 and energy fluxes of an Alaskan tussock tundra ecosystem," *Ecology*, vol. 80, no. 2, pp. 686–701, Mar. 1999.

[26] M. L. Goulden, S. C. Wofsy, J. W. Harden, S. E. Trumbore, P. M. Crill, S. T. Gower, T. Fries, B. C. Daube, S.-M. Fan, D. J. Sutton, A. Bazzaz, and J. W. Munger, "Sensitivity of boreal forest carbon balance to soil thaw," *Science*, vol. 279, no. 5348, pp. 214–217, Jan. 1998.

[27] M. Ueyama, Y. Harazono, E. Ohtaki, and A. Miyata, "Controlling factors on the interannual CO_2 budget at a subarctic black spruce forest in interior Alaska," *Tellus*, vol. 58, no. 5, pp. 491–501, Nov. 2006.

[28] A. G. Barr, T. A. Black, E. H. Hogg, T. J. Griffis, K. Morgenstern, N. Kljun, A. Theede, and Z. Nesic, "Climatic controls on the carbon and water balances of a boreal aspen forest, 1994–2003," *Glob. Change Biol.*, vol. 13, no. 3, pp. 561–576, Mar. 2006. DOI: 10.1111/j.1365-2486.2006.01220.x.

[29] L. B. Flanagan, L. A. Wever, and P. J. Carlson, "Seasonal and interannual variation in carbon dioxide exchange and carbon balance in a northern temperate grassland," *Glob. Change Biol.*, vol. 8, no. 7, pp. 599–615, Jul. 2002.

[30] Oak Ridge National Laboratory Distributed Active Archive Center (ORNL DAAC), *MODIS Subsetted Land Products, Collection 4*. (Accessed Jun. 12, 2006). [Online]. Available: http://www.daac.ornl.gov/MODIS/modis.html

[31] W. J. Parton, D. S. Schimel, C. V. Cole, and D. S. Ojima, "Analysis of factors controlling soil organic matter levels in Great Plains grasslands," *Soil Sci. Soc. Amer. J.*, vol. 51, pp. 1173–1179, 1987.

[32] T. Ise and P. R. Moorcroft, "The global-scale temperature and moisture dependencies of soil organic carbon decomposition: an analysis using a mechanistic decomposition model," *Biogeochemistry*, vol. 80, no. 3, pp. 217–231, Sep. 2006.

[33] C. S. Potter, J. T. Randerson, C. B. Field, P. A. Matson, and P. M. Vitousek, "Terrestrial ecosystem production: A process model based on global satellite and surface data," *Glob. Biogeochem. Cycles*, vol. 7, no. 4, pp. 811–841, 1993.

[34] C. M. Litton, J. W. Raich, and M. G. Ryan, "Carbon allocation in forest ecosystems," *Glob. Change Biol.*, vol. 13, no. 10, pp. 2089–2109, Jul. 2007.

[35] R. M. Gifford, "Plant respiration in productivity models: Conceptualization, representation, and issues for global terrestrial carbon-cycle research," *Funct. Plant Biol.*, vol. 30, no. 2, pp. 171–186, 2003.

[36] R. H. Waring, J. J. Landsberg, and M. Williams," Net primary production of forests: A constant fraction of gross primary production?" *Tree Physiol.*, vol. 18, no. 2, pp. 129–134, Feb. 1998.

[37] J. S. Amthor, "The McCree–de Wit–Penning de Vries–Thornley respiration paradigms: 30 years later," *Ann. Bot.*, vol. 86, no. 1, pp. 1–20, Jul. 2000.

[38] A. Mäkelä and H. T. Valentine, "The ratio of NPP to GPP: Evidence of change over the course of stand development," *Tree Physiol.*, vol. 21, no. 14, pp. 1015–1030, Sep. 2001.

[39] E. H. DeLucia, J. E. Drake, R. B. Thomas, and M. Gonzalez-Meler, "Forest carbon use efficiency: Is respiration a constant fraction of gross primary production?" *Glob. Change Biol.*, vol. 13, no. 6, pp. 1157–1167 Jun. 2007.

[40] W. Knorr, I. C. Prentice, J. I. House, and E. A. Holland, "Long-term sensitivity of soil carbon turnover to warming," *Nature*, vol. 433, no. 7023, pp. 298–301, Jan. 2005.

[41] J. Lloyd and J. A. Taylor, "On the temperature dependence of soil respiration," *Funct. Ecol.*, vol. 8, no. 3, pp. 315–323, Jun. 1994.

[42] F. F. Oberbauer, C. T. Gillespie, W. Cheng, R. Gebauer, A. Sala Serra, and J. D. Tenhunen, "Environmental effects on CO_2 efflux from riparian tundra in the northern foothills of the Brooks Range, Alaska, USA," *Oecologia*, vol. 92, pp. 568–577, 1992.

[43] C. J. Mikan, J. P. Schimel, and A. P. Doyle, "Temperature controls of microbial respiration in Arctic tundra soils above and below freezing," *Soil Biol. Biochem.*, vol. 34, no. 11, pp. 1785–1795, Nov. 2002.

[44] C. Fang and J. B. Moncrieff, "The dependence of soil CO_2 efflux on temperature," *Soil Biol. Biochem.*, vol. 33, no. 2, pp. 155–165, Feb. 2001.

[45] E. A. Davidson, L. V. Verchot, J. H. Cattânio, I. L. Ackerman, and J. E. M. Carvalho, "Effects of soil water content on soil respiration in forests and cattle pastures of eastern Amazonia," *Biogeochemistry*, vol. 48, no. 1, pp. 53–69, Jan. 2000.

[46] Y. Ino and M. Monsi, "An experimental approach to the calculation of CO_2 amount evolved from several soils," *Jpn. J. Bot.*, vol. 20, pp. 153–188, 1969.

[47] F. L. Bunnell and D. E. N. Tait, "Mathematical simulation models of decomposition processes," in *Soil Organisms and Decomposition in Tundra*, A. J. Holding, O. W. Heal, S. F. MacLean, Jr., and P. W. Flanagan, Eds. Stockholm, Sweden: Tundra Biome Steering Committee, 1974, pp. 207–225.

[48] S. F. Oberbauer, J. D. Tenhunen, and J. F. Reynolds, "Environmental effects on CO_2 efflux from water track and tussock tundra in Artic Alaska, U.S.A.," *Arct. Alp. Res.*, vol. 23, no. 2, pp. 162–169, May 1991.

[49] S. F. Oberbauer, W. Cheng, C. T. Gillespie, B. Ostendorf, A. Sala, G. Gebauer, R. A. Virginia, and J. D. Tenhunen, "Landscape patterns of carbon dioxide exchange in tundra ecosystems," in *Ecological Studies*, vol. 120, J. F. Reynolds and J. D. Tenhunen, Eds. Berlin, Germany: Springer-Verlag, 1996, pp. 223–256.

[50] D. P. Turner, W. D. Ritts, W. B. Cohen, S. T. Gower, M. Zhao, S. W. Running, S. C. Wofsy, S. Urbanski, A. L. Dunn, and J. W. Munger, "Scaling Gross Primary Production (GPP) over boreal and deciduous forest landscapes in support of MODIS GPP product validation," *Remote Sens. Environ.*, vol. 88, no. 3, pp. 256–270, Dec. 2003.

[51] D. P. Turner, W. D. Ritts, W. B. Cohen, S. T. Gower, S. W. Running, M. Zhao, M. H. Costa, A. A. Kirschbaum, J. M. Ham, S. R. Saleska, and D. E. Ahl, "Evaluation of MODIS NPP and GPP products across multiple biomes," *Remote Sens. Environ.*, vol. 102, no. 3/4, pp. 282–292, Jun. 2006.

[52] M. Zhao, F. A. Heinsch, R. R. Nemani, and S. W. Running, "Improvements of the MODIS terrestrial gross and net primary production global data set," *Remote Sens. Environ.*, vol. 96, no. 2, pp. 164–176, Mar. 2005.

[53] F. A. Heinsch, M. Zhao, S. W. Running, J. S. Kimball, R. R. Nemani *et al.*, "Evaluation of remote sensing based terrestrial productivity from MODIS using regional tower eddy flux network observations," *IEEE Trans Geosci. Remote Sens.*, vol. 44, no. 7, pp. 1908–1925, Jul. 2006.

[54] R. B. Myneni, S. Hoffman, Y. Knyazikhin *et al.*, "Global products of vegetation leaf area and fraction absorbed PAR from year one of MODIS data," *Remote Sens. Environ.*, vol. 83, no. 1, pp. 214–231, Nov. 2002.

[55] Data Assimilation Office (DAO), *Algorithm Theoretical Basis Document*, 2002, Greenbelt, MD: NASA Goddard Space Flight Center.

[56] Global Modeling and Assimilation Office (GMAO), *File Specification for GEOS-DAS Gridded Output Version 5.3, Report*, 2004, Greenbelt, MD: NASA Goddard Space Flight Center.

[57] P. Ashcroft and F. Wentz, "Algorithm theoretical basis document, AMSR level 2A algorithm," RSS, Santa Rosa, CA, Tech. Rep. 121 599B-1, 1999.

[58] E. G. Njoku, *AMSR Land Surface Parameters*. Pasadena, CA: Jet Propulsion Lab., 1999. ATBD 3.0. [Online]. Available: http://eospso.gsfc.nasa.gov/ftp_ATBD/REVIEW/AMSR/atbd-amsr-land.pdf

[59] E. G. Njoku, P. Ashcroft, T. K. Chan, and L. Li, "Global survey and statistics of radio-frequency interference in AMSR-E land observations," *IEEE Trans Geosci. Remote Sens.*, vol. 43, no. 5, pp. 938–947, May 2005.

[60] E. G. Njoku, *AMSR-E/Aqua Daily L3 Surface Soil Moisture, V001*. Boulder, CO: NSIDC, 2004. Digital Media.

[61] E. G. Njoku and S. K. Chan, "Vegetation and surface roughness effects on AMSR-E land observations," *Remote Sens. Environ.*, vol. 100, no. 2, pp. 190–199, Jan. 2006.

[62] W. Wagner, V. Naeimi, K. Scipal, R. de Jeu, and J. Martinez-Fernandez, "Soil moisture from operational meteorological satellites," *Hydrogeol. J.*, vol. 15, no. 1, pp. 121–131, Feb. 2007. DOI: 10.1007/s10040-006-0104-6.

[63] W. T. Crow and X. Zhan, "Continental-scale evaluation of remotely sensed soil moisture products," *IEEE Geosci. Remote Sens. Lett.*, vol. 4, no. 3, pp. 451–455, Jul. 2007.

[64] L. A. Jones, "Satellite microwave remote sensing of boreal–Arctic land surface state and meteorology from AMSR-E," "M.S. thesis," Univ. Montana, Missoula, MT, 2007.

[65] E. Falge, D. D. Baldocchi, R. Olson, P. Anthoni, M. Aubinet, C. Bernhofer, G. Burba, R. Ceulemans, R. Clement, H. Dolman, A. Granier, P. Gross, T. Grünwald, D. Hollinger, N.-O. Jensen, G. Katul, P. Keronen, A. Kowlaski, C. T. Lai, B. E. Law, T. Meyers, J. B. Moncrieff, E. Moors, J. W. Munger, K. Pilegaard, Ü. Rannik, C. Rebmann, A. Suyker, J. Tenhunen, K. Tu, S. Verma, T. Vesala, K. Wilson, and S. Wofsy, "Gap filling strategies for defensible annual sums of net ecosystem exchange," *Agric. For. Meteorol.*, vol. 107, no. 1, pp. 43–69, Mar. 2001.

[66] A. L. Dunn, C. C. Barford, S. C. Wofsy, M. L. Goulden, and B. C. Daube, "A long-term record of carbon exchange in a boreal black spruce forest: Means, responses to interannual variability, and decadal trends," *Glob. Change Biol.*, vol. 13, no. 3, pp. 577–590, Aug. 2007.

[67] A. R. Desai, P. V. Bolstad, B. D. Cook, K. J. Davis, and E. V. Carey, "Comparing net ecosystem exchange of carbon dioxide between an old-growth and mature forest in the upper Midwest, USA," *Agric. For. Meteorol.*, vol. 128, no. 1/2, pp. 33–55, Jan. 2005.

[68] B. D. Cook, K. J. Davis, W. Wang, A. Desai, B. W. Berger, R. M. Teclaw, J. G. Martin, P. V. Bolstad, P. S. Bakwin, C. Yi, and W. Heilman, "Carbon exchange and venting anomalies in an upland deciduous forest in northern Wisconsin, USA," *Agric. For. Meteorol.*, vol. 126, no. 3/4, pp. 271–295, Nov. 2004.

[69] A. R. Keyser, J. S. Kimball, R. R. Nemani, and S. W. Running, "Simulating the effects of climate change on the carbon balance of North American high-latitude forests," *Glob. Change Biol.*, vol. 6, no. 1, pp. 185–195, Dec. 2000.

[70] J. S. Kimball, P. E. Thornton, M. A. White, and S. W. Running, "Simulating forest productivity and surface–atmosphere carbon exchange in the BOREAS study region," *Tree Physiol.*, vol. 17, no. 8/9, pp. 589–599, Aug./Sep. 1997.

[71] J. S. Kimball, M. Zhao, A. D. McGuire, F. A. Heinsch, J. Clein, M. Calef, W. M. Jolly, S. Kang, S. E. Euskirchen, K. C. McDonald, and S. W. Running, "Recent climate-driven increases in vegetation productivity for the Western Arctic: Evidence of an acceleration of the northern terrestrial carbon cycle," *Earth Interact.*, vol. 11, no. 4, pp. 1–30, Feb. 2007.

[72] J. S. Amthor, J. Chen, J. Clein, S. Frolking, M. Goulden, R. Grant, J. Kimball, A. King, A. McGuire, N. Nikolov, C. Potter, S. Wang, and S. Wofsy, "Boreal forest CO_2 exchange and evapotranspiration predicted by nine ecosystem process models: Intermodel comparisons and relationships to field measurements," *J. Geophys. Res.*, vol. 106, no. D24, pp. 33 623–33 648, 2001.

[73] S. Kang, J. S. Kimball, and S. W. Running, "Simulating effects of fire disturbance and climate change on boreal forest productivity and evapotranspiration," *Sci. Total Environ.*, vol. 362, no. 1–3, pp. 85–102, Jun. 2006.

[74] P. E. Thornton, B. E. Law, H. L. Gholz, K. L. Clark, E. Falge, D. S. Ellsworth, A. H. Goldstein, R. K. Monson, D. Hollinger, M. Falk, J. Chen, and J. P. Sparks, "Modeling and measuring the effects of disturbance history and climate on carbon and water budgets in evergreen needleleaf forests," *Agric. For. Meteorol.*, vol. 113, no. 1/2, pp. 185–222, Dec. 2002.

[75] M. A. White, P. E. Thornton, S. W. Running, and R. R. Nemani, "Parameterization and sensitivity analysis of the BIOME-BGC terrestrial ecosystem model: Net primary production controls," *Earth Interact.*, vol. 4, no. 3, pp. 1–85, Jan. 2000.

[76] G. D. Farquhar and S. von Caemmerer, "Modelling of photosynthetic response to environmental conditions," in *Encyclopedia of Plant Physiology, New Series*, vol. 12B, O. L. Lange, P. S. Nobel, C. B. Osmond, and H. Ziegler, Eds. Berlin, Germany: Springer-Verlag, 1982, pp. 549–587.

[77] P. G. Jarvis and J. I. L. Morison, "Stomatal control of transpiration and photosynthesis," in *Stomatal Physiology*, P. G. Jarvis and T. A. Mansfield, Eds. Cambridge, U.K.: Cambridge Univ. Press, 1981, pp. 247–279.

[78] M. G. Ryan, "A simple method for estimating gross carbon budgets for vegetation in forest ecosystems," *Tree Physiol.*, vol. 9, pp. 255–266, 1991.

[79] M. A. White, P. E. Thornton, and S. W. Running, "A continental phenology model for monitoring vegetation responses to interannual climatic variability," *Glob. Biogeochem. Cycles*, vol. 11, no. 2, pp. 217–234, Jun. 1997.

[80] NOAA, *Summary of the Day—First Order (Data Set Documentation TD-3210)*, pp. 28801–5001, 2000, Asheville, NC: Nat. Climatic Data Center.

[81] S. W. Running, R. R. Nemani, and R. D. Hungerford, "Extrapolation of synoptic meteorological data in mountainous terrain and its use for simulating forest evapotranspiration and photosynthesis," *Can. J. For. Res.*, vol. 17, no. 6, pp. 472–483, 1987.

[82] P. E. Thornton and S. W. Running, "An improved algorithm for estimating incident daily solar radiation from measurements of temperature, humidity, and precipitation," *Agric. For. Meteorol.*, vol. 93, no. 4, pp. 211–228, Mar. 1999.

[83] Global Soil Data Task, *Global Soil Data Products CD-ROM (IGBP-DIS). International Geosphere–Biosphere Programme—Data and Information Services*, 2000, Oak Ridge, TN: ORNL Distributed Active Archive Center, Oak Ridge Nat. Lab. [Online]. Available: http://www.daac.ornl.gov/

[84] G. J. Michaelson, C. L. Ping, and J. M. Kimble, "Carbon storage and distribution in tundra soils of Arctic Alaska, U.S.A.," *Arct. Alp. Res.*, vol. 28, no. 4, pp. 414–424, Nov. 1996.

[85] G. J. Michaelson and C. L. Ping, "Soil organic carbon and CO_2 respiration at subzero temperature in soils of Arctic Alaska," *J. Geophys. Res.*, vol. 108, no. D2, p. 8164, 2003. DOI: 10.1029/2001JD000920.

[86] S. T. Gower, J. G. Vogel, J. M. Norman, C. J. Kucharik, S. J. Steele, and T. K. Stow, "Carbon distribution and aboveground net primary production in aspen, jack pine, and black spruce stands in Saskatchewan and Manitoba, Canada," *J. Geophys. Res.*, vol. 102, no. D24, pp. 29 029–29 041, 1997.

[87] J. G. Vogel, D. W. Valentine, and R. W. Ruess, "Soil and root respiration in mature Alaskan black spruce forests that vary in soil organic matter decomposition rates," *Can. J. For. Res.*, vol. 35, no. 1, pp. 161–174, Jan. 2005.

[88] S. E. Trumbore and J. W. Harden, "Accumulation and turnover of carbon in organic and mineral soils of the BOREAS northern study area," *J. Geophys. Res.*, vol. 102, no. D24, pp. 28 817–28 830, 1997.

[89] O. Bergeron, H. A. Margolis, T. A. Black, C. Coursolle, A. L. Dunn, A. G. Barr, and S. C. Wofsy, "Comparison of carbon dioxide fluxes over three boreal black spruce forests in Canada," *Glob. Change Biol.*, vol. 13, no. 1, pp. 89–107, Jan. 2007.

[90] G. Churkina and S. W. Running, "Contrasting climatic controls on the estimated productivity of global terrestrial biomes," *Ecosystems*, vol. 1, no. 2, pp. 206–215, Mar./Apr. 1998.

[91] J. S. Kimball, K. C. McDonald, S. W. Running, and S. E. Frolking, "Satellite radar remote sensing of seasonal growing seasons for boreal and subalpine evergreen forests," *Remote Sens. Environ.*, vol. 90, no. 2, pp. 243–258, Mar. 2004.

[92] J. B. Gaudinski, S. E. Trumbore, E. A. Davidson, and S. Zheng, "Soil carbon cycling in a temperate forest: Radiocarbon-based estimates of residence times, sequestration rates and partitioning of fluxes," *Biogeochemistry*, vol. 51, no. 1, pp. 33–69, 2000.
[93] E. A. G. Schuur and S. E. Trumbore, "Partitioning sources of soil respiration in boreal black spruce forest using radiocarbon," *Glob. Change Biol.*, vol. 12, no. 2, pp. 165–176, Feb. 2006.
[94] S. Trumbore, "Age of soil organic matter and soil respiration: Radiocarbon constraints on belowground C dynamics," *Ecol. Appl.*, vol. 10, no. 2, pp. 399–411, Apr. 2000.
[95] B. Bond-Lamberty, C. Wang, and S. T. Gower, "A global relationship between the heterotrophic and autotrophic components of soil respiration?" *Glob. Change Biol.*, vol. 10, no. 10, pp. 1756–1766, Oct. 2004.
[96] Y. Kim and N. Tanaka, "Effect of forest fire on the fluxes of CO_2, CH_4 and N_2O in boreal forest soils, interior Alaska," *J. Geophys. Res.*, vol. 108, no. D1, p. 8154, 2003. DOI: 10:1029/2001JD000663.
[97] A. D. Richardson, D. Y. Hollinger, J. D. Aber, S. V. Ollinger, and B. H. Braswell, "Environmental variation is directly responsible for short- but not long-term variation in forest–atmosphere carbon exchange," *Glob. Change Biol.*, vol. 13, no. 4, pp. 788–803, Apr. 2007.
[98] M. Aubinet, B. Heinesch, and B. Longdoz, "Estimation of the carbon sequestration by a heterogeneous forest: Night flux corrections, heterogeneity of the site and inter-annual variability," *Glob. Change Biol.*, vol. 8, no. 11, pp. 1053–1071, Sep. 2002.
[99] J. B. Moncrieff, Y. Malhi, and R. Leuning, "The propagation of errors in long-term measurements of land–atmosphere fluxes of carbon and water," *Glob. Change Biol.*, vol. 2, no. 3, pp. 231–240, Apr. 1996.
[100] E. Falge, D. Baldocchi, J. Tenhunen, M. Aubinet, P. Bakwin, P. Berbigier, C. Bernhofer, G. Burba, R. Clement, K. J. Davis, J. A. Elbers, A. H. Goldstein, A. Grelle, A. Granier, J. Guomundsson, D. Hollinger, A. S. Kowalski, G. Katul, B. E. Law, Y. Malhi, T. Meyers, R. K. Monson, J. W. Munger, W. Oechel, U. K. T. Paw, K. Pilegaard, U. Rannik, C. Rebmann, A. Suyker, R. Valenti, K. Wilson, and S. Wofsy, "Seasonality of ecosystem respiration and gross primary production as derived from FLUXNET measurements," *Agric. For. Meteorol.*, vol. 113, no. 1–4, pp. 53–74, Dec. 2002.
[101] M. Reichstein, E. Falge, D. Baldocchi, D. Papale, M. Aubinet, P. Berbigier, C. Bernhofer, N. Buchmann, T. Gilmanov, A. Granier, T. Grünwald, K. Havránková, H. Ilvesniemi, D. Janous, A. Knohl, T. Laurila, A. Lohila, D. Loustau, G. Matteucci, T. Meyers, F. Miglietta, J.-M. Ourcival, J. Pumpanen, S. Rambal, E. Rotenberg, M. Sanz, J. Tenhunen, G. Seufert, F. Vaccari, T. Vesala, D. Yakir, and R. Valentini, "On the separation of net ecosystem exchange into assimilation and ecosystem respiration: Review and improved algorithm," *Glob. Change Biol.*, vol. 11, no. 9, pp. 1424–1439, Sep. 2005.
[102] P. M. Lafleur and E. R. Humphreys, "Spring warming and carbon dioxide exchange over low Arctic tundra in central Canada," *Glob. Change Biol.*, vol. 14, no. 4, pp. 740–756, Dec. 2007.
[103] G. I. Ågren, E. Bosatta, and A. H. Magill, "Combining theory and experiment to understand effects of inorganic nitrogen on litter decomposition," *Oecologia*, vol. 128, no. 1, pp. 94–98, 2001.
[104] A. I. Hirsch, S. E. Trumbore, and M. L. Goulden, "Direct measurement of the deep soil respiration accompanying seasonal thawing of a boreal forest soil," *J. Geophys. Res.*, vol. 108, no. D3, p. 8221, 2003. DOI: 10.1029/2001JD000921.

John S. Kimball (M'08) received the B.A. and M.A. degrees in geography from San Diego State University, San Diego, CA, in 1987 and 1990, respectively, and the Ph.D. degree in bioresource engineering and geosciences from Oregon State University, Corvallis, in 1995.

He is an Associate Professor of biological sciences with The University of Montana (UM), Polson, where he is currently with the Flathead Lake Biological Station, Division of Biological Sciences. He is also with the Numerical Terradynamic Simulation Group, UM, Missoula. His research interests include the development and integration of biophysical theory with satellite remote sensing and computer modeling for understanding terrestrial ecosystem structure and function, from single plot to global scales.

Dr. Kimball is a member of NASA EOS MODIS and AMSR-E science teams and is working toward improved measurement and monitoring of global carbon and water cycles through the integration of ecological process models and satellite remote sensing.

Lucas A. Jones (S'06) received the B.Sc.(Hons.) and M.Sc. degrees in forestry with an emphasis in terrestrial ecology and remote sensing from The University of Montana (UM), Missoula, in 2005 and 2007, respectively, where he is currently working toward the Ph.D. degree in biology.

He is currently a Graduate Research Assistant with the Flathead Lake Biological Station, Division of Biological Sciences, UM, Polson, and also with the Numerical Terradynamic Simulation Group, UM, Missoula. He has previously worked with the USDA Forest Service Rocky Mountain Fire Sciences Laboratory, Missoula, and the Tongass National Forest, Ketchikan, AK. He has been a member of the American Geophysical Union since 2005. His research interests include passive microwave, radar, and optical remote sensing and biophysical modeling for studying carbon and water cycles at multiple temporal and spatial scales, particularly at high latitudes.

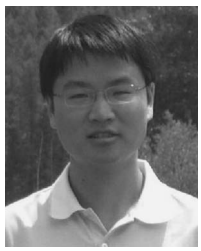

Ke Zhang received the B.S. and M.S. degrees in hydrology from Hohai University, Nanjing, China, in 2002 and 2005, respectively. He is currently working toward the Ph.D. degree in ecology at the University of Montana (UM), Missoula.

He is currently a Graduate Research Assistant with the Flathead Lake Biological Station, Division of Biological Sciences, UM, Polson, and also with the Numerical Terradynamic Simulation Group, UM, Missoula. His research interests include the remote sensing of terrestrial ecosystems, hydrological modeling, and ecological process modeling.

Faith Ann Heinsch received the M.S. degree in atmospheric sciences from Oregon State University, Corvallis, in 1997 and the Ph.D. degree in soil science from Texas A&M University, College Station, in 2002.

She is currently a Research Scientist with the Numerical Terradynamic Simulation Group, The University of Montana, Missoula. Her research interests include the study of soil–biosphere–atmosphere interactions, on the canopy to ecosystem scale using ecosystem models and remote sensing applications.

Kyle C. McDonald (S'79–M'83–SM'98) received the B.E.E. degree (cooperative plan with highest honors) from the Georgia Institute of Technology, Atlanta, in 1983, the M.S. degree in numerical science from Johns Hopkins University, Baltimore, MD, in 1985, and the M.S. and Ph.D. degrees in electrical engineering from The University of Michigan, Ann Arbor, in 1986 and 1991, respectively.

He has been with the Science Division, Jet Propulsion Laboratory, California Institute of Technology, Pasadena, since 1991, where he is currently a Research Scientist with the Water and Carbon Cycles Group. He specializes in electromagnetic scattering and propagation, with emphasis on microwave remote sensing of terrestrial ecosystems. His research interests primarily include the application of microwave remote sensing techniques for monitoring seasonal dynamics in boreal ecosystems, as related to ecological and hydrological processes and the global carbon and water cycles. He has been a Principal and Co-Investigator on numerous NASA Earth Science investigations. He is a member of NASA's North American Carbon Program (NACP) science team, NSF's Pan-Arctic Community-wide Hydrological Analysis and Monitoring Program (Arctic-CHAMP) Science Steering Committee, and the ALOS PALSAR Kyoto & Carbon Initiative science panel. He has been a member of the NASA BOREAS and BOREAS Follow-on science teams, the NASA Scatterometer instrument team, the NASA Ocean Vector Winds Science Team, and the NASA Cold Land Processes Steering Committee.

Walt C. Oechel received the B.A. degree from San Diego State University, San Diego, CA, in 1966 and the Ph.D. degree from the University of California, Riverside, in 1970.

He is a Professor of biology with San Diego State University, where he is the Director of the Global Change Research Group, Department of Biology.